

Aemulus ν : Precision halo mass functions in $w\nu$ CDM cosmologies

Delon Shen^{a,b} Nickolas Kokron^{c,d} Joseph DeRose^e Jeremy Tinker^f Risa H. Wechsler^{a,b} Arka Banerjee^g and the Aemulus Collaboration

^aDepartment of Physics, Stanford University, 382 Via Pueblo Mall, Stanford, CA 94305, USA

^bKavli Institute for Particle Astrophysics and Cosmology, SLAC National Accelerator Laboratory, 2575 Sand Hill Road, Menlo Park, CA 94025, USA

^cDepartment of Astrophysical Sciences, Princeton University, 4 Ivy Lane, Princeton, NJ, 08544, USA

^dSchool of Natural Sciences, Institute for Advanced Study, 1 Einstein Drive, Princeton, NJ, 08540, USA

^ePhysics Division, Lawrence Berkeley National Laboratory, 1 Cyclotron Rd, Berkeley, CA, USA

^fCenter for Cosmology and Particle Physics, Department of Physics, New York University, 726 Broadway, New York, NY 10003, USA

^gDepartment of Physics, Indian Institute of Science Education and Research, Homi Bhabha Road, Pashan, Pune 411008, India

E-mail: delon@stanford.edu, kokron@astro.princeton.edu, jderose@lbl.gov, tinker@nyu.edu, rwechsler@stanford.edu, arka@iiserpune.ac.in

Abstract. Precise and accurate predictions of the halo mass function for cluster mass scales in $w\nu$ CDM cosmologies are crucial for extracting robust and unbiased cosmological information from upcoming galaxy cluster surveys. Here, we present a halo mass function emulator for cluster mass scales ($\gtrsim 10^{13}M_{\odot}/h$) up to redshift $z = 2$ with comprehensive support for the parameter space of $w\nu$ CDM cosmologies allowed by current data. Based on the Aemulus ν suite of simulations, the emulator marks a significant improvement in the precision of halo mass function predictions by incorporating both massive neutrinos and non-standard dark energy equation of state models. This allows for accurate modeling of the cosmology dependence in large-scale structure and galaxy cluster studies. We show that the emulator, designed using Gaussian Process Regression, has negligible theoretical uncertainties compared to dominant sources of error in future cluster abundance studies. Our emulator is [publicly available](#), providing the community with a crucial tool for upcoming cosmological surveys such as LSST and Euclid.

Contents

1	Introduction	1
2	Measuring the Halo Mass Function from N-body Simulation	3
2.1	The Aemulus ν Simulation Suite	3
2.2	Measuring the Mass Function	3
2.3	Fitting the Mass Function	4
2.4	Fits Performance	9
3	Design of Halo Mass Function Emulator	9
3.1	Brief Review of Gaussian Process Regression	9
3.2	Specifications of our Gaussian Process Emulator	10
3.3	Emulator Performance	13
4	Emulator Error Quantification and Accuracy Requirement	13
4.1	Theoretical Systematic Uncertainty on Cluster Abundance due to Emulator	13
4.2	Comparison to Systematic Uncertainty in Mass-Observable Calibration	15
5	Conclusion	17
A	Cosmology Dependence of the Halo Mass Function in Low and High $S8$ Cosmologies	18
B	Complete Performance Plots	18

1 Introduction

The next several years will see a new suite of large cosmological surveys designed to measure the growth of structure and expansion history of the universe and thus probe cosmological parameters, including the evolution of dark energy, the impact of dark matter, and the role of massive neutrinos at significantly higher precision. These surveys promise to provide unprecedented data on galaxy clusters, which, as the most massive virialized structures in the universe, provide a unique window into the high-mass, exponentially suppressed tail of the halo mass function [1–14]. For example, current observations of galaxy clusters with optical surveys like the Dark Energy Survey (DES) [15–18], Hyper Suprime-Cam [19, 20], and Kilo-Degree Survey (KiDS) [21] as well as observations of X-ray emission [22–27], and the thermal Sunyaev–Zel’dovich effects [28–35] provide measurements of thousands of galaxy clusters. As this number increases dramatically in the era of LSST, Euclid, and the Simons Observatory [6, 36–38], theoretical models must evolve to match the increasing accuracy of observations. In particular, the cosmology dependence of the halo mass function across a wide range of cosmological parameters that account for massive neutrinos and non-standard dark energy models must be precisely calibrated to ensure that theoretical uncertainties remain a negligible source of error and to extract robust and unbiased cosmological information that makes full use of the data.

The halo mass function, which predicts the comoving number density of dark matter halos in a given mass range, has been a cornerstone of cosmological theory since the spherical

collapse model was first used to estimate it in the early work of Ref. [39]. This analytic prediction was further formalized in Ref. [40] with the excursion set approach. In these analytic predictions, the halo mass function’s dependence on cosmology and redshift was contained primarily within a measure of a halo’s rarity: the peak height. In other words, the mass function was predicted to be “universal”. Over the years, refinements based on increasingly accurate N -body simulations have characterized the dependence of the mass function on cosmological parameters [41–48], and also have revealed deviations from universality [49–55]. This non-universality must be explicitly accounted for, especially in the context of upcoming surveys, which will rely on precise modeling of the halo mass function to derive cosmological constraints from cluster abundance data.

Non-universality in the halo mass function can be tackled numerically by building an *emulator*. Generically, an emulator for a summary statistic is constructed by interpolating between measurements of that summary statistic from a set of sufficiently accurate simulations that carefully sample the desired parameter space. Once built, the emulator can take input parameters (like cosmology and redshift) and produce predictions for the target statistic with a clear estimate of uncertainty. Emulators have successfully been constructed for several non-linear summary statistics such as the matter power spectrum [56–61], linear halo bias [62, 63], galaxy clustering and lensing statistics [61, 64–71], higher-order statistics [72–74], and most importantly for this paper, the halo mass function [62, 75, 76].

Building on these foundational studies, here we present a new halo mass function emulator for cluster mass scales $\gtrsim 10^{13}M_{\odot}/h$ and up to redshift $z = 2$, with comprehensive support for the full range of $w\nu$ CDM cosmologies allowed by current data. Built on the **Aemulus** ν suite of N -body simulations outlined in Ref. [61], our emulator marks a significant improvement in precision by incorporating both massive neutrinos and non-standard dark energy models. By using Gaussian Process Regression [77] to predict halo abundances, we show that the theoretical uncertainties of the emulator are negligible compared to dominant sources of error in upcoming galaxy cluster abundance studies. This accuracy of the emulator ensures that its errors remain subdominant for future large-scale cosmological surveys, such as LSST and Euclid. Following the analytical derivations of the halo mass function in Refs. [39, 40], we express the fitting function in terms of the linear matter power spectrum. This allows the linear matter power spectrum to capture most of the cosmology and redshift dependence of the halo mass function, leaving only the residual non-universal cosmology and redshift dependence to the emulation step.

The rest of this paper is organized as follows. Sec. 2 reviews the details of the **Aemulus** ν suite of simulations and describes how we measure and subsequently fit the halo mass function in each simulation. Sec. 3 describes the design and training of our Gaussian process emulator and verifies its accuracy. We explore the cosmology dependence of the halo mass function in low and high S8 cosmologies using our emulator in App. A. In Sec. 4, we construct a model for the theoretical systematic uncertainty introduced by our emulator and demonstrate that this uncertainty due to our emulator will be negligible compared to dominant systematic uncertainties for cluster abundance studies using data from up to LSST Y10. We conclude in Sec. 5.

2 Measuring the Halo Mass Function from N -body Simulation

2.1 The Aemulus ν Simulation Suite

Cluster cosmology probes halos in the exponentially suppressed high-mass tail of the halo mass function. To model this regime precisely, we need N -body simulations with enough resolution and volume to ensure we have a sufficient number of high-mass halos to consider. This work uses the **Aemulus ν** suite of 150 simulations run in a $w\nu$ CDM cosmological parameter space [61]. We specify each simulation in this suite with cosmological parameters

$$\Omega = \{10^9 A_s, n_s, H_0, w_0, \Omega_b h^2, \Omega_c h^2, \Sigma m_\nu\}, \quad (2.1)$$

where the parameters are

- $10^9 A_s$: amplitude of scalar fluctuations,
- n_s : scalar spectral index,
- H_0 : Hubble constant,
- w_0 : dark energy equation of state,
- $\Omega_b h^2$: baryon density,
- $\Omega_c h^2$: cold dark matter density, and
- Σm_ν : sum of neutrino masses.

These simulations are run over a broad parameter space, ensuring that emulators constructed using this suite are accurate over the full range of $w\nu$ CDM cosmologies allowed by current data. Each simulation has a side length of $L = 1050 h^{-1} \text{Mpc}$, and jointly evolves the CDM–baryon field (‘cb’) and the neutrino field, with $N = 1400^3$ particles for each species. This corresponds to a cb particle mass of $3.5 \times 10^{10} \left(\frac{\Omega_{\text{cb}}}{0.3}\right) h^{-1} M_\odot$. This suite of simulations also employs a two-tiered parameter-space design. The second tier of 50 simulations, sampled with a Sobol sequence [78], densely samples the $w\nu$ CDM cosmologies currently allowed by the combinations (1) DES Y3 weak lensing and galaxy clustering+BAO+type Ia supernovae and (2) Planck 2018+BAO+type Ia supernovae. The first tier of 100 simulations, sampled using a Latin hypercube, spans a broader parameter space. Each simulation is initialized at $z = 12$, which is significantly later in cosmic time than previously possible, by using third-order Lagrangian perturbation theory [79, 80]. Doing this mitigates bias in force calculations due to discreteness effects in the particle distribution [79]. We refer the reader to Ref. [61] for more details on this suite of simulations.

2.2 Measuring the Mass Function

In this paper, we define halo mass as 200 times the background CDM + baryon density:

$$\text{Halo Mass Definition: } M_{200\text{cb}} = 200 \times \text{background CDM + baryon density}. \quad (2.2)$$

When estimating the halo mass, we count all particles within $R_{200\text{cb}}$ of the halo, even if they are not bound to it. Namely, these are “strict spherical overdensity” masses. We identify halos with the **ROCKSTAR** halo finder [81] in 15 redshift snapshots between $z = 0$ and $z \approx 2.3$.

For a given snapshot, we bin by mass the identified halos that do not lie within $R_{200\text{cb}}$ of a more massive halo. Namely, we consider only host halos and ignore subhalos. The mass binning is started at $\log_{10}(200 \times M_{\text{particle}})$ rounded up to the nearest tenth. For example, if a given box has $\log_{10}(200 \times M_{\text{particle}}) = 12.85$ we start the mass binning at $\log_{10} M = 12.9$. We then set the bin width so that we have ten bins per decade:

$$\text{Mass Bin Width : } \Delta \log_{10} M = 0.1. \quad (2.3)$$

After this, we merge the final mass bins associated with the most massive halos until the final mass bin has at least 20 halos¹. Then, each mass bin is assigned a “true mass” corresponding to the mean mass of halos put into that mass bin. Let us define the array of measured number counts in all the redshift snapshots of a specified box as

$$\mathbf{N}_{\text{true}}(\text{Box}) : \begin{array}{l} \text{Array of measured number counts in all redshift snapshots of a} \\ \text{specified box.} \end{array} \quad (2.4)$$

Once we have measured the mass function for a box at redshift z , we can estimate the covariance between mass bins at a fixed redshift for this box using 32^3 spatial jackknife subvolumes. Jackknifing estimates our measurements’ sample variance and shot noise [82]. We neglect estimating covariance between mass bins in different redshift snapshots. Let us define the Jackknifed covariance matrix for measured number counts in all redshift snapshots of a given box as

$$\mathbf{K}_{\mathbf{N}_{\text{true}}}(\text{Box}) : \begin{array}{l} \text{Jackknifed covariance matrix between measured number counts in} \\ \text{all redshift snapshot of a specified box.} \end{array} \quad (2.5)$$

2.3 Fitting the Mass Function

We fit the measured abundances \mathbf{N}_{true} with the functional form of the mass function proposed in Appendix C of Ref. [52] modified to depend only on the CDM and baryon mass density field ρ_{cb} as opposed to the whole matter content of CDM, baryons, and massive neutrinos:

$$\frac{dn(M, z)}{dM} = G(\sigma_{\text{cb}}(M, z)) \frac{\bar{\rho}_{\text{cb},0}}{M} \frac{d \ln \{ \sigma_{\text{cb}}(M, z)^{-1} \}}{dM}. \quad (2.6)$$

This modification to only consider the CDM and baryon content is required because neutrinos do not cluster on halo scales and thus do not contribute to the collapse of dark matter halos [83–85]. $\bar{\rho}_{\text{cb},0}$ is the mean CDM and baryon mass density at $z = 0$,

$$\rho_{\text{cb},0} = \frac{3H_0^2}{8\pi G} (\Omega_c + \Omega_b), \quad (2.7)$$

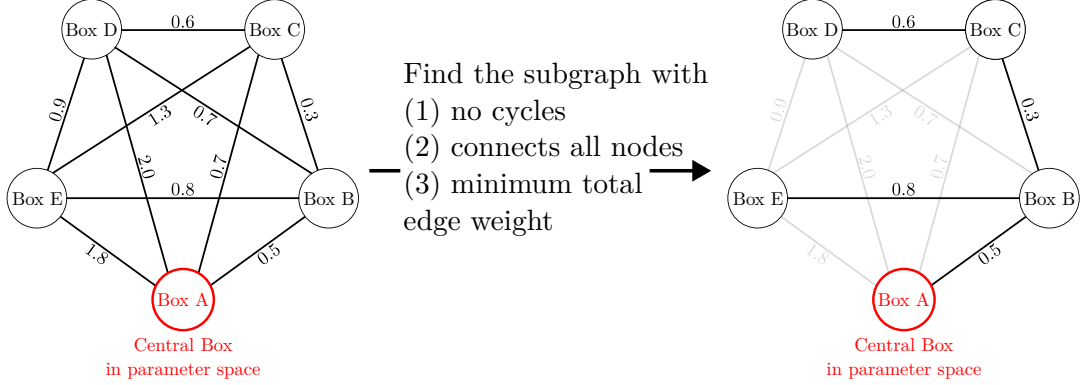
and σ_{cb}^2 is the variance of the CDM+baryon density field ρ_{cb} smoothed on the Lagrangian radius $R_L = (3M/4\pi\bar{\rho}_{\text{cb},0})^{1/3}$ associated with a mass M :

$$\sigma_{\text{cb}}^2(R_L[M], z) = \int d \ln k \frac{k^3 P_{\text{cb,lin}}(k, z)}{2\pi^2} |\hat{W}(kR_L)|^2. \quad (2.8)$$

¹We neglect redshift snapshots with < 20 halos that have mass $> 200 \times M_{\text{particle}}$. In our entire suite of simulations, we neglected only a single redshift snapshot of a single tier 1 simulation.

Build Tree from position of boxes in νCDM parameter space

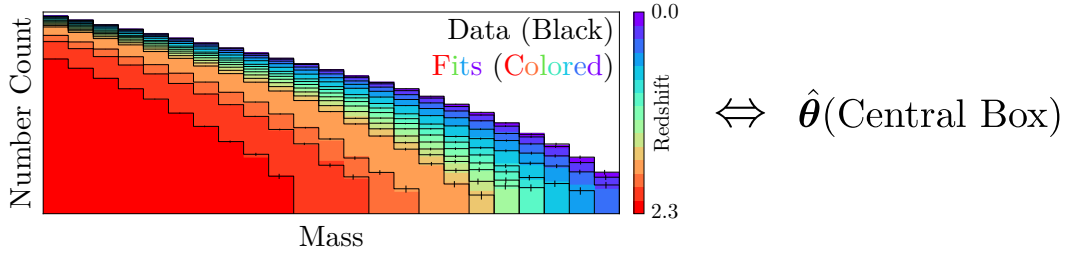
Edge Weight \sim distance between two boxes in νCDM parameter space



Whole suite has 150 boxes. Showing 5 for simplicity

Fit Halo Mass Function of Central Box

Let $\hat{\theta}$ be the parameters of our fitting function for the halo mass function



Use $\hat{\theta}(\text{Central Box})$ to seed the iterative fitting of the simulation suite

Let $A \rightarrow B$ denote using $\hat{\theta}(A)$ as a prior for $\hat{\theta}(B)$

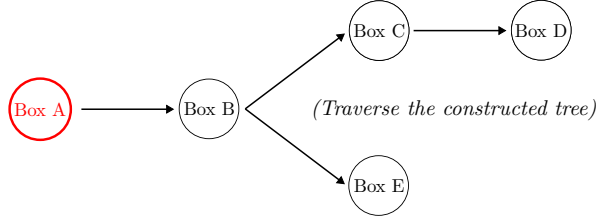


Figure 1. Visualization of our iterative fitting procedure, described in detail in Sec. 2.3.

$P_{\text{cb,lin}}(k, z)$ is the linear CDM and baryon power spectrum and \hat{W} is the Fourier transform of the spatial top-hat filter

$$\hat{W}(x) = 3 \frac{\sin(x) - x \cos(x)}{x^3}. \quad (2.9)$$

We compute both σ_{cb} and $P_{\text{cb,lin}}$ with the Boltzmann code CLASS [86, 87]. The halo multiplicity function $G(\sigma_{\text{cb}})$ is defined as

$$G(\sigma_{\text{cb}}) = B \left[\left(\frac{\sigma_{\text{cb}}}{e} \right)^{-d} + \sigma_{\text{cb}}^{-f} \right] \exp(-g/\sigma_{\text{cb}}^2). \quad (2.10)$$

Refs. [43, 45] presented similar fitting functions. In the halo model, all dark matter lives in a halo [88]. Asserting this leads to the normalization

$$\int d \ln \sigma^{-1} G(\sigma) = 1. \quad (2.11)$$

This normalization allows us to write B in terms of the remaining free parameters of the halo mass function:

$$B = 2 \left[e^d g^{-d/2} \Gamma\left(\frac{d}{2}\right) + g^{-f/2} \Gamma\left(\frac{f}{2}\right) \right]^{-1}, \quad (2.12)$$

where $\Gamma(z)$ is the generalized factorial or Gamma function.

We can compute the halo abundance predicted by Eq. (2.6), $\hat{\mathbf{N}}$, that is suitable to directly compare with the halo abundances we measure from our boxes \mathbf{N}_{true} from Eq. (2.4) by integrating Eq. (2.6) in each mass bin and multiplying by the comoving volume of our box V_{box} :

$$\hat{N} = V_{\text{box}} \int_{\text{bin}}^{\text{mass}} \frac{dn}{dM}(M) dM. \quad (2.13)$$

If we fix the values of $\{d, e, f, g\}$, then Eq. (2.6) is a universal mass function. Our emulator will incorporate non-universality by allowing the parameters $\{d, e, f, g\}$ to vary smoothly as a function of cosmology and redshift. This allows us to naturally combine the cosmology and redshift dependence of the physically motivated functional form Eq. (2.6) while allowing the smooth variation of $\{d, e, f, g\}$ to capture the residual non-universality.

To assert that $\{d, e, f, g\}$ depends smoothly on the cosmological parameters and scale factor, we adopt an iterative fitting approach summarized in Fig. 1. Let $\mathbf{X} \sim \mathcal{N}(\boldsymbol{\mu}, \mathbf{K})$ mean that \mathbf{X} is n -dimensional Gaussian random vector with mean $\boldsymbol{\mu}$ and covariance matrix \mathbf{K} :

$$\mathbf{X} \sim \mathcal{N}(\boldsymbol{\mu}, \mathbf{K}) \Leftrightarrow P(\mathbf{X}) = \sqrt{\frac{1}{(2\pi)^n \times \det[\mathbf{K}]}} \exp\left\{-\frac{1}{2}(\mathbf{X} - \boldsymbol{\mu})^T \mathbf{K}^{-1}(\mathbf{X} - \boldsymbol{\mu})\right\}. \quad (2.14)$$

First, to assert that each $p \in \{d, e, f, g\}$ depends smoothly on scale factor a for a given cosmology $\boldsymbol{\Omega}$ we specify a linear dependence on the scale factor:

$$p(\boldsymbol{\Omega}, a) = p_0(\boldsymbol{\Omega}) + (a - 0.5)p_1(\boldsymbol{\Omega}). \quad (2.15)$$

We found this to be a good approximation for the redshift evolution of $\{d, e, f, g\}$ by individually fitting the parameters in each redshift snapshot and observing a linear dependence. So, when fitting our suite of simulations, we fit the mass function from all redshift snapshots of a given simulation simultaneously. Thus, for a given simulation, the parameters we fit are

$$\boldsymbol{\theta} = \{d_0, d_1, e_0, e_1, f_0, f_1, g_0, g_1\}. \quad (2.16)$$

In general, $\boldsymbol{\theta}$ are chosen to maximize the posterior

$$P(\boldsymbol{\theta} | \hat{\mathbf{N}}; \text{Box}) \propto P(\boldsymbol{\theta}; \text{Box}) \times P(\hat{\mathbf{N}} | \boldsymbol{\theta}; \text{Box}), \quad (2.17)$$

where we build the likelihood using Eqs. (2.4) and (2.5):

$$(\hat{\mathbf{N}} | \boldsymbol{\theta}; \text{Box}) \sim \mathcal{N}(\mathbf{N}_{\text{true}}(\text{Box}), \mathbf{K}_{\mathbf{N}_{\text{true}}}(\text{Box})). \quad (2.18)$$

The prior $P(\boldsymbol{\theta}; \text{Box})$ is what we will vary as we go through our iterative fitting.

To start our iterative fitting, we fit parameters of the mass function θ of our central-most box in cosmological parameter space. For this central-most box, we first fit the $z = 0$ snapshot by setting $d = 1.97^2$ to fix degeneracies and finding $\{e, f, g\}$ that maximize the likelihood Eq. (2.18). We then use these parameters fit from the $z = 0$ snapshot to fix one endpoint of the linear dependence Eq. (2.15) of the parameters and fit θ to all redshift snapshots with the prior that

$$\{p(\Omega, a) \mid p \in \{d, e, f, g\}\} \geq 0. \quad (2.19)$$

By maximizing the posterior Eq. (2.17) with this prior, we have the fitted parameters $\hat{\theta}(\text{Central Box})$. We then use the fitted $\hat{\theta}(\text{Central Box})$ as a prior on the mass function parameters for fitting the next closest few boxes to the central most box

$$\theta(\text{Nearly Central Box}) \sim \mathcal{N}(\hat{\theta}(\text{Central Box}), \mathbf{K}_\theta). \quad (2.20)$$

We will formally define ‘‘Nearly Central Box’’ and similar terminology shortly. The parameters for a given nearly central box $\hat{\theta}(\text{Nearly Central Box})$ are then used as a prior in the same way as $\hat{\theta}(\text{Central Box})$. Namely, it is used as a prior on the mass function parameters for fitting the next closest few boxes to this Nearly Central Box:

$$\theta(\text{Near Nearly Central Box}) \sim \mathcal{N}(\hat{\theta}(\text{Nearly Central Box}), \mathbf{K}_\theta) \quad (2.21)$$

This process continues iteratively until we have fit the mass function for all simulations in our suite. We empirically find that

$$\mathbf{K}_\theta = \text{diag}(10^{-2}, 10^{-2}, 10^{-3}, 10^{-3}, 5 \times 10^{-4}, 5 \times 10^{-4}, 10^{-4}, 10^{-4}) \quad (2.22)$$

is sufficiently relaxed to achieve a sound fit but restrictive enough to wrangle degeneracies between our mass function parameters.

It is left to formalize which boxes are ‘‘nearly central boxes’’ and ‘‘near nearly central box’’ and so on. To do this, we construct a graph of our boxes to traverse as follows:

1. Standardize each $w\nu\text{CDM}$ cosmological parameters so that each simulation is labeled with parameters that have comparable characteristic spread (mean zero and unit variance):

$$\omega' \equiv \frac{\omega - \langle \omega \rangle}{\sqrt{\langle \omega^2 \rangle - \langle \omega \rangle^2}} \quad \forall \omega \in \{w\nu\text{CDM Cosmological Parameters (Eq. (2.1))}\}. \quad (2.23)$$

2. Build a fully connected graph where each box is a node and edges between two boxes are weighted by the distance in standardized parameter space between those two boxes:

$$\text{EdgeWeight}(\text{Box A}, \text{Box B}) = \sqrt{(\omega'(\text{Box A}) - \omega'(\text{Box B}))^2} \quad (2.24)$$

3. Find the subset of this fully connected graph centered on the central-most box in cosmological parameter space that has no cycles, connects all nodes together, and has the minimum total edge weight³.

Thus, we have constructed a graph that formalizes what we mean by ‘‘nearly central boxes’’ and so on that we can traverse through to iteratively fit our whole suite of simulations.

²this specific choice of $d = 1.97$ is motivated by Table 4 of Ref. [52]

³Formally this is known as a minimum spanning tree for which there are well-established algorithms for efficiently finding such a subset [89–93].

Residuals of the Halo Mass Function **Fits** (Tier 2)

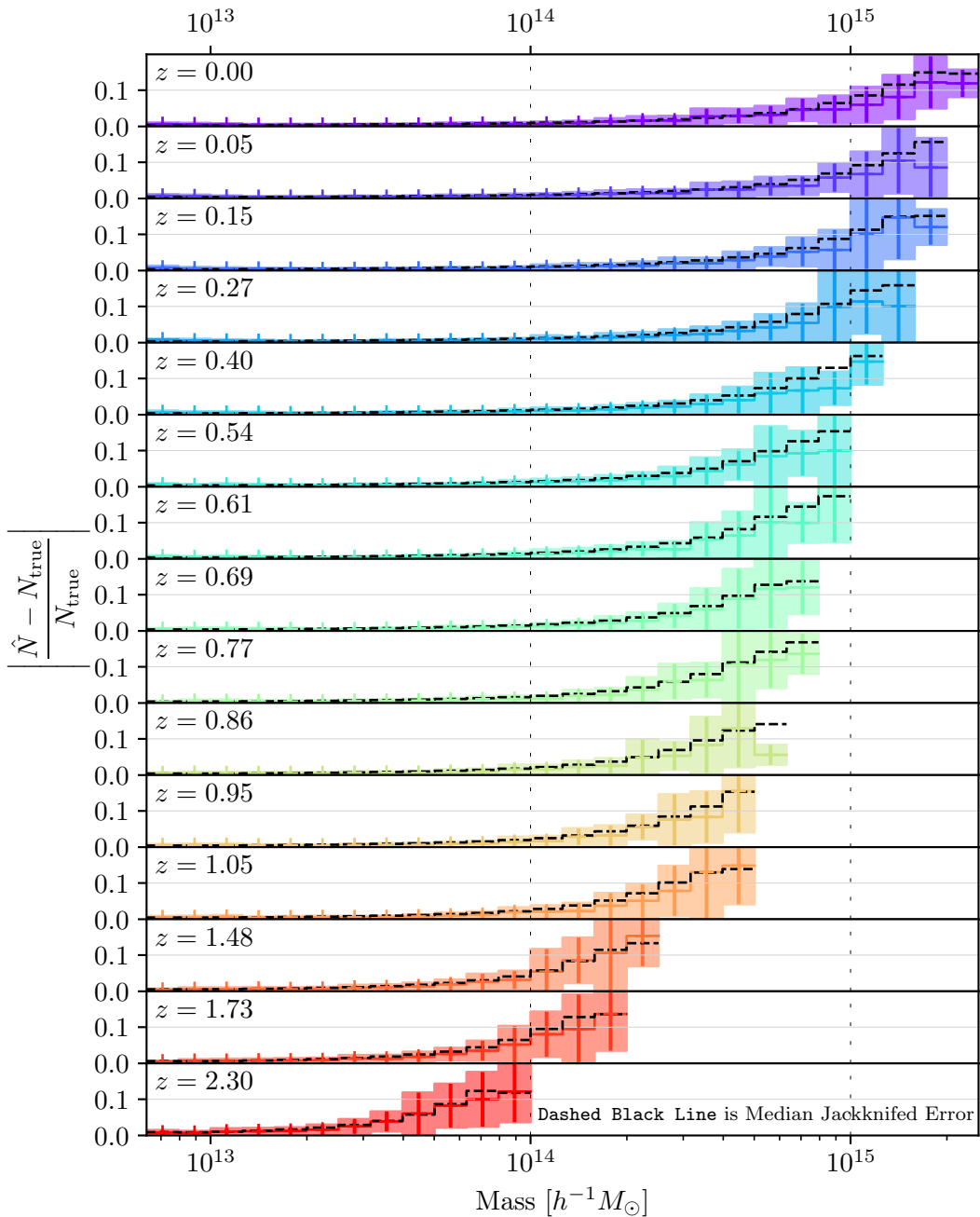


Figure 2. The absolute fractional error on halo abundance from our fits (colored) compared to the median jackknifed error (dashed black) in a given mass bin indicates that for currently allowed $w\nu$ CDM cosmologies (tier 2 simulations), the error in abundance from our fits is dominated by the inherent shot noise and sample variance. Bands correspond to $\pm 1\sigma$ from the mean.

2.4 Fits Performance

To evaluate the performance of our fitting scheme, we plot in Fig. 2 the absolute fractional error of the fits versus the actual measured mass function for currently allowed $w\nu$ CDM cosmologies (tier 2 simulations)⁴. To guide the eye, we plot the median jackknife error in a bin in dashed black. By comparing the fractional errors of our fits with the median jackknife error, we find that the error resulting from the methodology described in Sec. 2.3 is dominated by shot noise and sample variance.

3 Design of Halo Mass Function Emulator

Our emulator uses a Gaussian process (GP), thoroughly treated in Ref. [77], to predict the parameters of the fitting function θ (Eq. (2.16)) as a function of cosmological parameters (Eq. (2.1)).

3.1 Brief Review of Gaussian Process Regression

First recall from Eq. (2.14) a n -dimensional Gaussian random vector

$$\mathbf{Y} = [Y_1, Y_2, \dots, Y_n] \sim \mathcal{N}(\boldsymbol{\mu}, \mathbf{K}) \quad (3.1)$$

with mean matrix $\boldsymbol{\mu} = [\mu_1, \dots, \mu_n]$ and covariance matrix \mathbf{K} whose elements we will call K_{ij} . For a Gaussian random vector, if we marginalize over any subset of its constituent random variables $\mathbf{Y}^* \subset \mathbf{Y}$, then the remaining $\mathbf{Y}' \equiv \{Y_i \notin \mathbf{Y}^*\}$ will still be described by a Gaussian random vector:

$$\mathbf{Y}' \sim \mathcal{N}(\boldsymbol{\mu}', \mathbf{K}'), \quad (3.2)$$

where \mathbf{K}' is the relevant submatrix of \mathbf{K} and $\boldsymbol{\mu}'$ is the relevant subvector of $\boldsymbol{\mu}$. We have chosen to index the random variables Y_i , which make up \mathbf{Y} with integers: $i \in [1, 2, \dots, n]$. However, we could have just as easily indexed them with fractions: $i \in [\frac{1}{n}, \frac{2}{n}, \dots, 1]$. In that case, the mean matrix and covariance matrix are also appropriately relabelled $\boldsymbol{\mu} = [\mu_{1/n}, \mu_{2/n}, \dots, \mu_1]$ and $K_{i/n, j/n}$. We can take the $n \rightarrow \infty$ limit, in which case it would be more appropriate to describe our collection of random variables, Y_i , as a scalar function $y(x)$, which is defined for $x \in (0, 1]$. Correspondingly, the mean and covariance would be more appropriately described as functions $\mu(x)$ and $K(x, x')$. This defines a Gaussian process, which we denote as

$$Y \sim \mathcal{N}(\mu(x), K(x, x')) \quad (3.3)$$

The property Eq. (3.2) generalizes to the statement that any finite number of random variables from our infinite collection of random variables $Y(x)$ are described by a Gaussian random vector. For example, a vector of random variables like $[Y(x_1), Y(x_2)]$ is still described by a Gaussian random vector:

$$\begin{bmatrix} Y(x_1) \\ Y(x_2) \end{bmatrix} \sim \mathcal{N} \left(\begin{bmatrix} \mu(x_1) \\ \mu(x_2) \end{bmatrix}, \begin{bmatrix} K(x_1, x_1) & K(x_1, x_2) \\ K(x_2, x_1) & K(x_2, x_2) \end{bmatrix} \right). \quad (3.4)$$

This property is the key that enables the use of GPs for regression. In this example, $x \in (0, 1]$ but it is possible to define a GP on an arbitrary interval.

⁴We show the equivalent plot on the whole suite of simulations in App. B

Now, we schematically describe how GPs are used for regression. Suppose at positions $\mathbf{x} = [x_1, x_2, \dots, x_n]$ we can measure⁵ the output of a function we wish to fit, $f(x)$. One could then assume that $f(\mathbf{x})$ is drawn from a Gaussian random vector that is a subset of a Gaussian process:

$$f(\mathbf{x}) \sim \mathcal{N}(0, \mathbf{K}_{\mathbf{q}}) \subset f \sim \mathcal{N}(0, k_{\mathbf{q}}(x, x')), \quad (3.5)$$

where without loss of generality, we have subtracted off the mean so that the GP is centered at zero. \mathbf{K} is determined by the kernel function $k_{\mathbf{q}}(x, x')$ with free parameters \mathbf{q} whose goal is to capture the character of $f(x)$, the function we're fitting:

$$\mathbf{K}_{\mathbf{q},ij} = k_{\mathbf{q}}(x_i, x_j) \quad (3.6)$$

For example if we had measured $f(x)$ at two point $\mathbf{x} = [x_1, x_2]$ then we could say

$$f(\mathbf{x}) \sim \mathcal{N}\left(\mathbf{0}, \begin{bmatrix} k_{\mathbf{q}}(x_1, x_1) & k_{\mathbf{q}}(x_1, x_2) \\ k_{\mathbf{q}}(x_2, x_1) & k_{\mathbf{q}}(x_2, x_2) \end{bmatrix}\right), \quad (3.7)$$

analogous to Eq. (3.4). Thus, the parameters of this method of fitting $f(x)$ are the parameters of the kernel function \mathbf{q} . These parameters are determined by maximizing the likelihood

$$\arg \max_{\mathbf{q}} \left(-\frac{1}{2} f(x_i) (\mathbf{K}_{\mathbf{q}}^{-1})_{ij} f(x_j) - \frac{1}{2} \ln(\det[\mathbf{K}_{\mathbf{q}}]) + \text{const.} \right) \quad (3.8)$$

where repeated indices are summed over. In essence, the success of using GPs for regression boils down to the kernel function's ability to capture the character of the function we are fitting. From here, if we wish to predict f at some points \mathbf{x}_* , then we can draw a sample from the Gaussian random vector

$$(f(\mathbf{x}_*) \mid \mathbf{x}, f(\mathbf{x}), \mathbf{x}_*) \sim (\text{GP at some points } \mathbf{x}_* \mid \text{GP} = \text{the data } f(\mathbf{x}) \text{ at points } \mathbf{x}) \quad (3.9)$$

where we refer the reader to Ref. [77] for the explicit form of this distribution. Though we have focused on GP regression for the simplest 1D case with no measurement noise, the generalization to multiple input and noisy measurements is possible and again discussed in Ref. [77].

3.2 Specifications of our Gaussian Process Emulator

The input of our Gaussian process is the cosmological parameters specifying each box Eq. (2.1). To stabilize the training of our Gaussian process, we normalize the inputs so that each input lies between 0 and 1:

$$\omega' \equiv \frac{\omega - \min(\omega)}{\max(\omega) - \min(\omega)} \quad \forall \omega \in \{w\nu\text{CDM Cosmological Parameters (Eq. (2.1))}\}. \quad (3.10)$$

Let's first focus on fitting the cosmology and redshift dependence for one of the mass function parameters $t \in \boldsymbol{\theta}$. From Sec. 2, we have $n = 150$ measurement of this parameter at different cosmologies. We can use these measurements⁶ to model the cosmology dependence of the parameter $t \in \boldsymbol{\theta}$ using a Gaussian process as schematically described in Sec. 3.1.

⁵Generally, we would also assume each measurement has some measurement error ϵ . For this simple discussion, we shall neglect this for clarity.

⁶To train the GP, we treat these measurements as "noiseless" measurements

As discussed there, the choice of kernel is a critical component in specifying our model. A popular choice for the kernel is the squared-exponential kernel with parameters \mathbf{q} where $k_{\mathbf{q}}(\mathbf{x}, \mathbf{x}') \sim \exp\{-\sum_i (x_i - x'_i)^2 / \ell_i^2\}$. In our emulator, we instead choose to use a more expressive kernel built primarily around the Matérn kernel [77, 94, 95]:

$$k_{\mathbf{q}}^{(\Omega)}(\mathbf{x}, \mathbf{x}') = A \times \frac{2^{1-\nu}}{\Gamma(\nu)} \left(\frac{|\mathbf{x} - \mathbf{x}'|}{C} \times \sqrt{2\nu} \right)^\nu K_\nu \left(\frac{|\mathbf{x} - \mathbf{x}'|}{C} \times \sqrt{2\nu} \right) + B \quad (3.11)$$

where $\Gamma(\nu)$ is the Gamma function and K_ν is the modified Bessel function of the second kind. We have chosen the smoothness parameter $\nu = 1/2$. The free parameters are the scaling parameters A and C as well as the additive constant to the kernel B :

$$\mathbf{q} = \{A, B, C\}. \quad (3.12)$$

We also model the mean of the Gaussian process as linear in the inputs

$$\mu_{\{\mathbf{w}, b\}}(\Omega) = \mathbf{w} \cdot \Omega + b \quad (3.13)$$

where $\{\mathbf{w}, b\}$ are the free parameters for this mean model. Thus, we have specified the architecture of a GP emulator for one mass function parameter as a function of cosmology.

To properly construct a GP emulator that can simultaneously model all the (correlated) mass function parameters θ in Eq. (2.16), we use the framework presented in Ref. [96] which extends the covariance in Eq. (3.11) to include covariances between two mass function parameters $t, t' \in \theta$, $k_{\mathbf{q}'}^{(\theta)}(t, t')$:

$$k_{\{\mathbf{q}, \mathbf{q}'\}}([\mathbf{x}, t], [\mathbf{x}', t']) = k_{\mathbf{q}}^{(\Omega)}(\mathbf{x}, \mathbf{x}') \otimes k_{\mathbf{q}'}^{(\theta)}(t, t') \quad (3.14)$$

where \otimes denotes the Kronecker product and $k_{\mathbf{q}'}^{(\theta)}$ is a lookup table with parameters \mathbf{q}' that contains the halo mass function parameter covariances. We model this lookup table as

$$k_{\mathbf{q}'}^{(\theta)}(t, t') = (\mathbf{D}\mathbf{D}^T + \text{diag}(\mathbf{v}))_{t, t'} \quad (3.15)$$

where \mathbf{D} is a matrix of rank 1 and \mathbf{v} is a non-negative vector. The free parameters for the covariance between mass function parameters are thus

$$\mathbf{q}' = \{\mathbf{D}, \mathbf{v}\}. \quad (3.16)$$

We also model the mean for each mass function parameter $t \in \theta$ as linear in the inputs

$$\mu_{\{\mathbf{w}^{(t)}, b^{(t)}\}}(\Omega) = \mathbf{w}^{(t)} \cdot \Omega + b^{(t)} \quad \forall t \in \theta \quad (\text{Eq. (2.16)}) \quad (3.17)$$

where $\{\mathbf{w}^{(t)}, b^{(t)} \mid t \in \theta\}$ are the free parameters for this mean model. Thus, we have specified the architecture of a GP emulator for all the correlated mass function parameters as a function of cosmology.

We “train” the GP specified by Eqs. (3.14) and (3.17)⁷, e.g., determine the free parameters $\{\mathbf{q}, \mathbf{q}', \mathbf{w}^{(t)}, b^{(t)}\}$ of our GP emulator’s mean and kernel components, by maximizing the generalization of likelihood described in Eq. (3.8). When training the GP, we use the iterative AdamW optimization algorithm [98] to maximize the likelihood. The AdamW optimizer is first run with a learning rate of 0.01 for 500 iterations and then decreased to a learning rate of 0.001 for another 500 iterations. This training procedure then provides an emulator of the halo mass function parameter as a function of cosmology.

⁷To train our model, we use the `gpytorch` Gaussian Process library [97] but make our final public emulator independent of `gpytorch` by extracting the trained parameters and using them with our own minimal Gaussian Process library that is constructed to make predictions only.

Residuals of the Halo Mass Function **Emulator** (Tier 2)

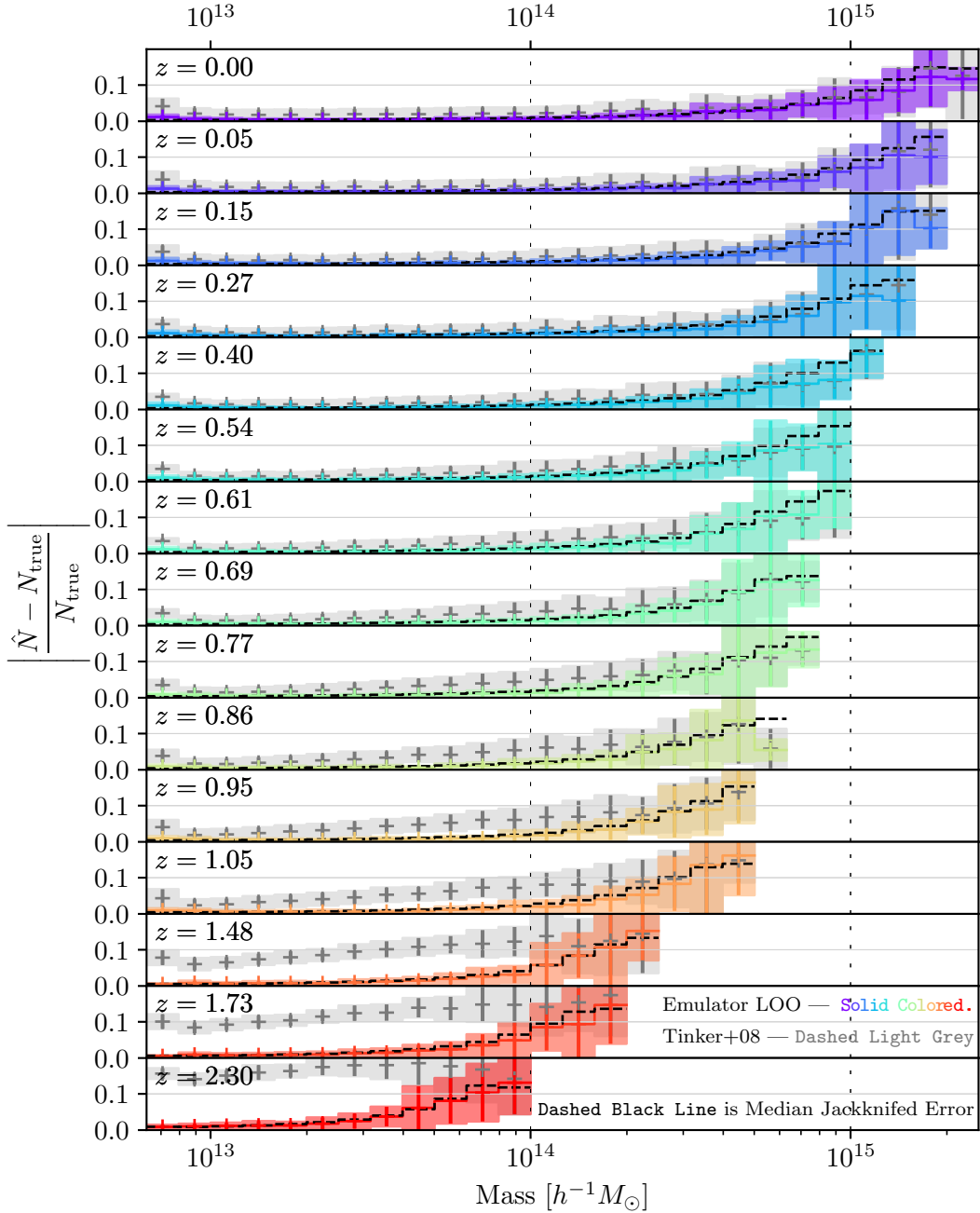


Figure 3. The absolute fractional error on halo abundance for a given box from our emulator architecture trained on all but that box (colored) when compared to (1) the median jackknifed error (dashed black) and (2) the error of the Tinker halo mass function modified to depend only on CDM and baryons [83–85] (light grey). This indicates that in currently allowed $w\nu$ CDM cosmologies, (1) the error in abundance from our emulator is dominated by shot noise and sample variance, and (2) our emulator is significantly more accurate and precise than the Tinker mass function combined with prescriptions that adapt it to $w\nu$ CDM cosmologies. We quantitatively model the theoretical systematic error on cluster abundances due to our emulator in Sec. 4 and show in Fig. 5 that our emulator is sufficiently precise and accurate to be a subleading source of uncertainty in upcoming cluster abundance surveys. Bands correspond to $\pm 1\sigma$ from the mean.

3.3 Emulator Performance

To evaluate the performance of our emulator, we plot in Fig. 3 the absolute fractional error between the prediction of an emulator trained on all but one box versus the measured abundances Eq. (2.4) of that left out box $|(\hat{\mathbf{N}}_{\text{loo}} - \mathbf{N}_{\text{true}})/\mathbf{N}_{\text{true}}|$ for currently allowed $w\nu$ CDM cosmologies (tier 2 simulations)⁸. To guide the eye, we also plot (1) the median jackknifed shot noise and sample variance in a given mass bin as a dashed black line and (2) the absolute fractional error when using the Tinker halo mass function presented in Ref. [52] modified to depend only on the CDM and baryon content as described Sec. 2.3 and Refs. [83–85] in light grey. We find that the error of our emulator, similar to the error of the fits shown in Fig. 2, is dominated by shot noise and sample variance, meaning additional theoretical uncertainty introduced by our fitting and emulation is negligible. We quantitatively characterize the theoretical systematic uncertainty on halo abundances due to our emulator in Sec. 4 and show it will be negligible compared to dominant systematic uncertainties for upcoming cluster abundance studies. Furthermore, by comparing the colored and the light grey bands, we see that in $w\nu$ CDM cosmologies currently allowed by data, our halo mass function emulator is significantly more accurate and precise than the standard Tinker mass function [52] with prescriptions that adapt it to $w\nu$ CDM cosmologies [83–85]. In addition to the decreased precision and accuracy of the Tinker mass function, we also find that the Tinker mass function’s response to cosmological parameters differs from our emulator depending on which fiducial cosmology is chosen (Figs. 6 and 7). We explore the implications of this for non-universality more fully in App. A.

4 Emulator Error Quantification and Accuracy Requirement

In surveys, clusters are binned as a function of some observable, e.g., redMaPPer richness [99], X-ray luminosity [100], or CMB flux decrement due to the Sunyaev-Zel’dovich effect [101]. The mean cluster mass in an observable bin is then determined through some relation between mass and cluster observable. This relation can be calibrated with several techniques, one of the most powerful being weak lensing [6, 102–108]. Generically, this calibration allows us to measure the mean mass of an observable bin $\ln M$ with some uncertainty $\sigma_{\ln M}$. This uncertainty from the mass-observable calibration leads to an uncertainty in the cluster abundance. So, a reasonable accuracy requirement for our halo mass function emulator is that its contribution to uncertainty in cluster abundance is negligible compared to the uncertainty introduced from the mass-observable calibration for upcoming surveys. In this section, we first build a model for the theoretical systematic uncertainty on cluster abundances due to our halo mass function emulator. We then demonstrate that this theoretical systematic uncertainty due to our emulator is negligible compared to uncertainty from weak lensing mass-observable calibration for up to LSST Y10 data.

4.1 Theoretical Systematic Uncertainty on Cluster Abundance due to Emulator

Following Ref. [75], we model the theoretical systematic uncertainty in abundance measurements due to our emulator $\sigma_{\log N|_{\text{mf}}}$ as a power law:

$$\sigma_{\log N|_{\text{mf}}}(M, a) = A + B \times \exp\{C \times [\nu(M, a) - 3] + D \times [a - 0.5]\}, \quad (4.1)$$

⁸We show the equivalent plot on the whole suite of simulations in App. B

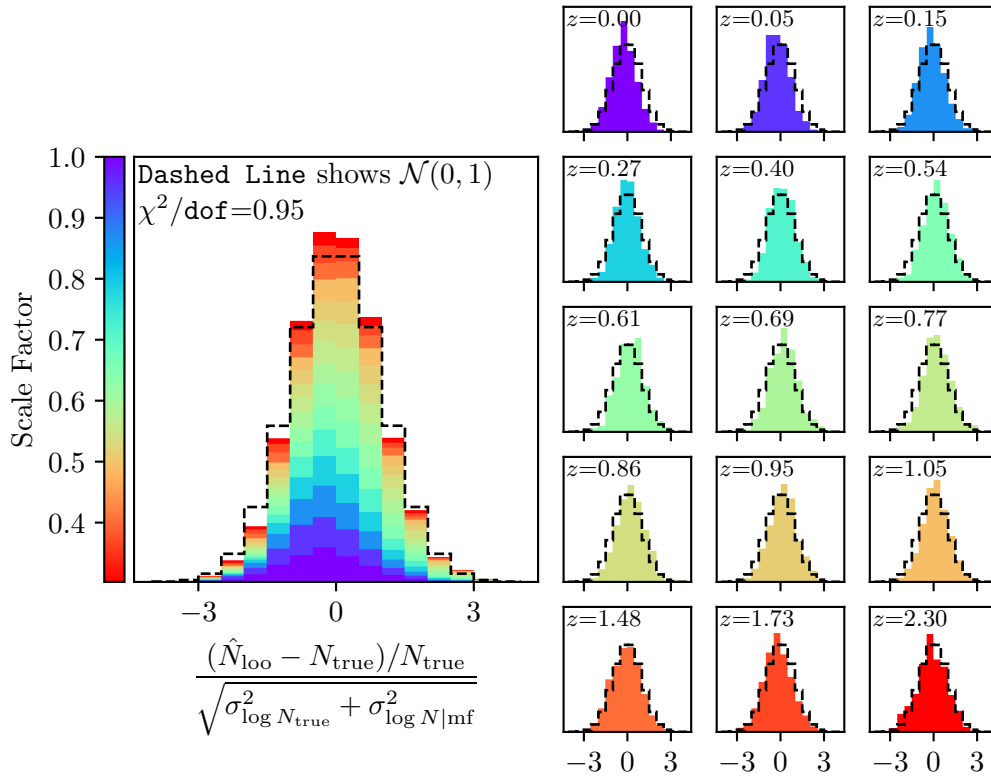


Figure 4. Model of the theoretical systematic uncertainty due to our emulator, $\sigma_{\log N|mf}^2$ from Sec. 4 (colored). The model closely matches that expected for a perfect model of the emulator error (dashed black) when jointly considering residuals in all redshift snapshots in the set of tier 2 simulations (left) but contains minor pathologies when considering a fixed redshift (right).

where a is the scale factor and $\nu(M, a)$ is the peak height:

$$\nu(M, a) = \frac{\delta_c}{\sigma_{cb}(M, a)}. \quad (4.2)$$

Here, $\delta_c = 1.686$ is the linear collapse threshold for an Einstein de-Sitter cosmology, and $\sigma_{cb}(M, a)$ is the variance of the smoothed CDM and baryon field described in Eq. (2.8). The fitting parameters of σ_{mf} are $\{A, B, C, D\}$. The fractional residuals in the leave-one-out test shown in Fig. 3 are due to a sum in quadrature of (1) sample variance and shot noise, estimated by jackknifing, $K_{N_{true}}$ (Eq. (2.5)), and (2) some additional theoretical systematic uncertainty due to the mass function, $\sigma_{\log N|mf}$. So we can model the total covariance matrix of the fractional residuals $K_{frac.res.}$ as

$$K_{frac.res.} = \frac{K_{N_{true}}}{N_{true} \otimes N_{true}} + K_{\log N|mf} \equiv K_{\log N_{true}} + K_{\log N|mf}, \quad (4.3)$$

where

$$K_{\log N|mf} = \text{diag}(\sigma_{\log N|mf}^2(M_1, a), \sigma_{\log N|mf}^2(M_2, a), \dots), \quad (4.4)$$

	$A [h^{-1}M_{\odot}]^{1.5}$	$n_0 [\text{arcmin}^{-2}]$	z_*
DES Y6	0.7×10^{22}	8.4	0.6
LSST Y1	0.7×10^{22}	10	0.85
LSST Y10	0.7×10^{22}	27	0.85

Table 1. Parameters used in Sec. 4.2 for our model of the dominant systematic uncertainty from stacked weak lensing mass calibration, the shape noise, taken from Refs. [75, 109].

and M_i is the mean mass of halos in the i^{th} mass bin. We can fit for $\{A, B, C, D\}$ by modelling the fractional residual in the leave-one-out test shown in Fig. 3 as

$$\left(\frac{\hat{\mathbf{N}}_{\text{loo}} - \mathbf{N}_{\text{true}}}{\mathbf{N}_{\text{true}}} \middle| \{A, B, C, D\} \right) \sim \mathcal{N}(0, \mathbf{K}_{\text{frac.res.}}). \quad (4.5)$$

Maximizing the above likelihood provides a model for the theoretical systematic uncertainty in abundance measurements due to our emulator.

In Fig. 4, we plot the distribution of fractional residuals in the leave-one-out test divided by the jackknifed shot noise and sample variance plus our best-fit error model added in quadrature. A perfect error model would yield a normal distribution with unit variance, plotted as a dashed line. We find that when jointly considering residuals in all redshift snapshots in currently allowed $w\nu\text{CDM}$ cosmologies, our error model yields a distribution that is nearly a Gaussian with unit variance and acceptable reduced χ^2 value of $\chi^2/\text{dof} = 0.95$.

4.2 Comparison to Systematic Uncertainty in Mass-Observable Calibration

We now compute the cluster abundance uncertainty due to weak lensing mass-observable calibration, $\sigma_{\log N|\text{calib.}}$. The abundance in a given mass bin can be written as

$$\log N = \Delta \log M \frac{d \log N}{d \log M} \quad (4.6)$$

where as in Eq. (2.3) we have $\Delta \log_{10} M = 0.1$ or 10 mass bins per decade. If the bin has a true mass $\log M_b$ but we measure this true mass with some uncertainty $\sigma_{\log M}$, then we can Taylor expand to find the error in abundance due to error in the mass calibration:

$$\begin{aligned} \log N(\log M_b + \sigma_{\log M}) &= \Delta \log M \frac{d \log N}{d \log M} \bigg|_{\log M_b + \sigma_{\log M}} \\ &\approx \Delta \log M \left(\frac{d \log N}{d \log M} + \sigma_{\log M} \frac{d^2 \log N}{d \log M^2} \right) \bigg|_{\log M_b} \\ &= \log N_{\text{true}} + \sigma_{\log M} \Delta \log M \frac{d^2 \log N}{d \log M^2} \bigg|_{\log M_b} \end{aligned} \quad (4.7)$$

From this, we can read off the error in abundance due to an error in the mass-observable calibration, $\sigma_{\log N|\text{calib.}}$, as

$$\sigma_{\log N|\text{calib.}} = \sigma_{\log M} \times \Delta \log M \frac{d^2 \log N}{d \log M^2} \bigg|_{\log M_b} \quad (4.8)$$

The dominant source of uncertainty for weak lensing measurements of galaxy cluster masses comes from the intrinsic distribution of galaxy shapes within a catalog [107]. This intrinsic

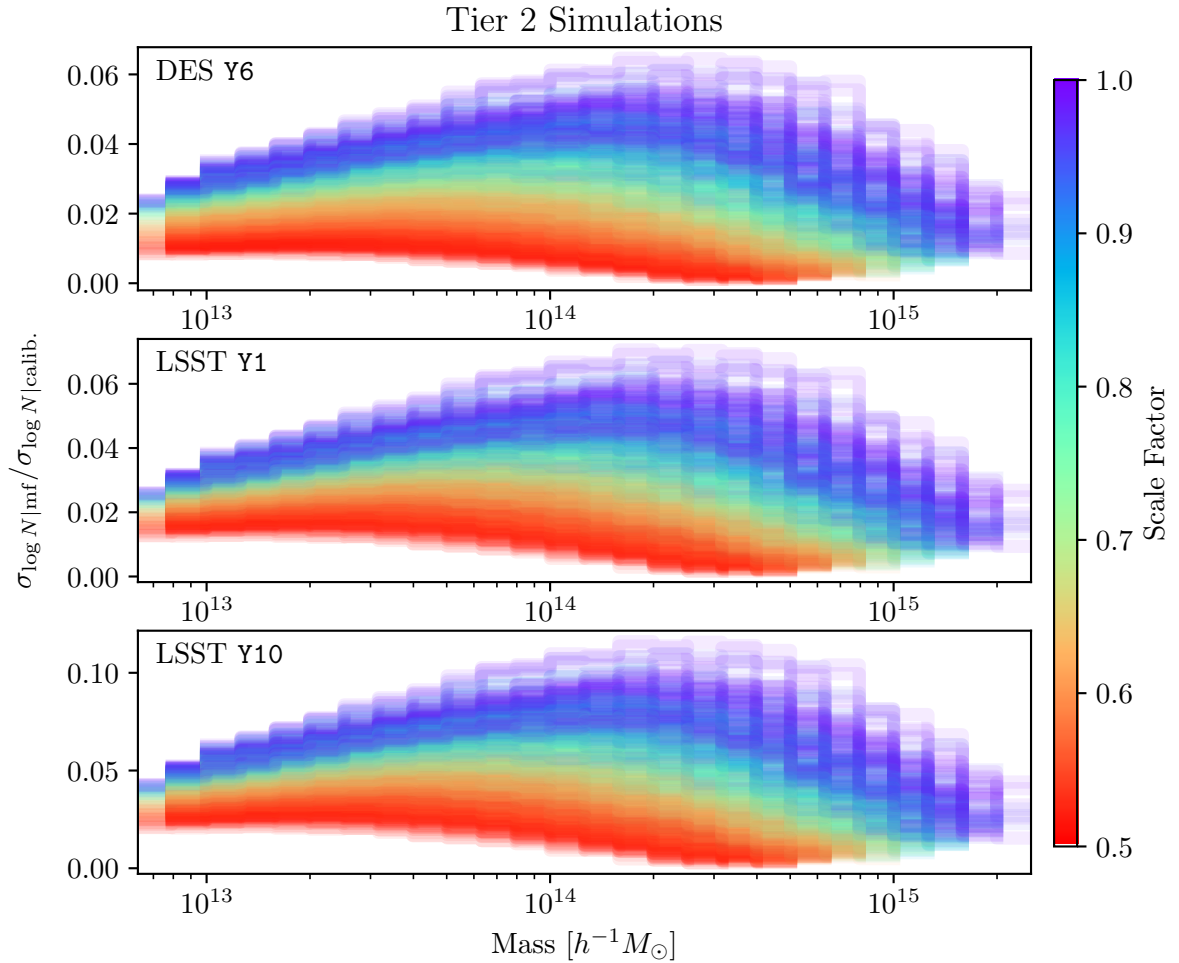


Figure 5. Emulator error compared to the calibration error in the observable–mass relation. In cluster abundance studies, the dominant systematic uncertainty in abundance measurements arises from observable–mass relations, which must be calibrated. This calibration introduces some uncertainty $\sigma_{\log N|\text{calib.}}$. Here, we show that the uncertainty on abundances due to our emulator $\sigma_{\log N|\text{mf}}$ is significantly subleading to uncertainties from weak lensing mass-observable calibration for current and upcoming studies. From top to bottom, the panels show the ratio of these errors in DES Y6 (imminent analysis), LSST Y1 (analysis expected in a few years), and LSST Y10 (note the different y-axis in the final panel).

variation is called *shape noise*. So, we approximate the mass–observable calibration uncertainty from weak lensing $\sigma_{\log M}$ as being due only to shape noise⁹:

$$\sigma_{\log M} = \sigma_{\log M}^{\text{SN}} = \frac{\sigma_M^{\text{SN}}}{M}. \quad (4.9)$$

⁹Note that this is more stringent than Ref. [75], which approximates the mass–observable calibration uncertainty from weak lensing as being due to shape noise (like is done here) *and* scatter in mass at fixed richness.

Following Ref. [75] we model shape noise as

$$(\sigma_M^{\text{SN}})^2 = AM^{1/2}(N_c n)^{-1}. \quad (4.10)$$

In the above, N_c is the number of clusters, A is a constant, and n is the lensing source density. As we go to higher redshift, lenses have fewer sources behind them to lens. Thus, our estimate of their masses will become increasingly noisy. This redshift dependence of $\sigma_{\log M}$ comes in as a redshift dependence of the lensing source density n , which we model as

$$n(z) \approx n_0 \times \exp\left\{-\frac{1}{2} \frac{z^2}{z_*^2}\right\}, \quad (4.11)$$

where z_* is the characteristic redshift where local source density peaks. All together, we have

$$(\sigma_M^{\text{SN}})^2 = \frac{AM^{1/2}}{N_c} \frac{6.3 \text{ arcmin}^{-2}}{n_0} \exp\left\{-\frac{1}{2} \frac{z^2}{z_*^2}\right\}. \quad (4.12)$$

The numerical values of the parameters of this noise model are taken from Refs. [75, 109] and are tabulated in Table 1.

In Fig. 5, we show that theoretical systematic uncertainty in cluster abundances due to our emulator is significantly smaller than uncertainty due to weak lensing mass-observable calibration for up to LSST Y10 data. Thus, theoretical systematic uncertainty due to our halo mass function emulator will be a negligible source of error for upcoming cluster abundance studies.

5 Conclusion

Precision predictions of the halo mass function in $w\nu$ CDM cosmologies are crucial for extracting robust cosmological information from upcoming galaxy cluster surveys. In this paper, we have presented a halo mass function emulator suitable for cluster mass scales $M_{200b} \gtrsim 10^{13} M_\odot/h$ and redshifts $z \leq 2$ for a broad range of $w\nu$ CDM cosmologies. The emulator is constructed with the **Aemulus** ν suite of N -body simulations which span the broadest $w\nu$ CDM parameter space ever used in a single suite of simulations. We use a fitting function for the halo mass function presented in Ref. [52] modified to depend on only the CDM and baryon components [83–85] to fit the measured halo abundances in each simulation in this suite. A Gaussian process is then trained on the measured parameters of this fitting function to predict the cosmology dependence of these parameters. This design allows us to naturally combine the inherent cosmology and redshift dependence of universal halo mass functions derived from physically motivated models while directly capturing residual non-universality through the Gaussian process. We find (Fig. 3) that for currently allowed $w\nu$ CDM cosmologies, our emulator is significantly more accurate and precise than the Tinker mass function [52] combined with prescriptions that adapt it to $w\nu$ CDM cosmologies [83–85]. We quantify the theoretical systematic uncertainty on cluster abundances due to our halo mass function emulator. This is compared with uncertainties due to weak lensing mass-observable calibration from DES Y6, LSST Y1, and LSST Y10 data. We find (Fig. 5) that the theoretical systematic uncertainty on cluster abundances due to our emulator will be negligible compared to uncertainty due to mass-observable calibration for upcoming cluster abundance studies. We make our emulator for the halo mass function [publicly available](#) and encourage its use in future cosmological analyses.

Acknowledgments

We thank Federico Bianchini, Adam Mantz, Emmanuel Schaan, and Chun-Hao To for helpful discussions. This work received support from the U.S. Department of Energy under contract number DE-AC02-76SF00515 to SLAC National Accelerator Laboratory. D.S. is additionally supported by the National Science Foundation Graduate Research Fellowship under Grant No. DGE-2146755. J.D. is supported by the Lawrence Berkeley National Laboratory Chamberlain Fellowship. JT is supported by National Science Foundation grant 2009291. This research used resources of the National Energy Research Scientific Computing Center, a DOE Office of Science User Facility supported by the Office of Science of the U.S. Department of Energy under Contract No. DE-AC02-05CH11231. Some of the computing for this project was performed on the Sherlock cluster. We thank Stanford University and the Stanford Research Computing Center for providing computational resources and support that contributed to these research results. This work used Stampede2 at the Texas Advanced Computing Center and Bridges2 at the Pittsburgh Supercomputing Center through allocation PHY200083 from the Extreme Science and Engineering Discovery Environment (XSEDE) [110], which was supported by National Science Foundation grant number 1548562.

A Cosmology Dependence of the Halo Mass Function in Low and High S8 Cosmologies

In a high S8 (Planck [111]) cosmology, the cosmology dependence of the halo mass function on cluster mass scales, shown in Fig. 6, changes significantly between the universal Tinker halo mass function modified to depend only on the CDM and baryon content as described Sec. 2.3 and Refs. [83–85] and our non-universal halo mass function emulator. Most notable is the change in the character of n_s dependence¹⁰. This differs from a low S8 (DES Y3 [114]) cosmology where the cosmology dependence of the halo mass function on cluster mass scales, shown in Fig. 7, changes less between the universal Tinker halo mass function and our non-universal halo mass function emulator in comparison to a high S8 cosmology. This difference between low and high S8 cosmologies occurs because there are more clusters in a high S8 cosmology. Thus, the halo mass function has a greater dynamic range for cluster mass scales, which allows for increased cosmology dependence and impact from non-universality.

B Complete Performance Plots

In this appendix, we show the performance plots of our fits and emulator for the whole suite of simulations instead of only the tier 2 simulations. As described in Sec. 2.1, the Aemulus ν suite of simulations employs a two-tiered parameter space design. The primary tier of interest is tier 2, which spans the range of $w\nu$ CDM cosmologies allowed by current data. Namely, (1) DES Y3 weak lensing and galaxy clustering+BAO+type Ia supernovae and (2) Planck 2018+BAO+type Ia supernovae. So, these are the cosmologies where the accuracy

¹⁰The fact that changes in the spectral index n_s capture a significant amount of non-universality is not a new idea in the literature. For example, Ref. [112] found that an analogous quantity, the local power spectrum slope defined as the slope of $\sigma(R)$ at the Lagrangian radius of a halo of mass M , was a primary driver of non-universality. However, later on, Ref. [113] found that neither the local slope of the power spectrum nor n_s played any significant role in non-universality for the halo mass function at $z = 0$ and instead utilized deep learning to identify three other variables that are necessary and sufficient to predict the HMF at $z = 0$ to sub percent accuracy.

High S8 (Planck) Cosmology

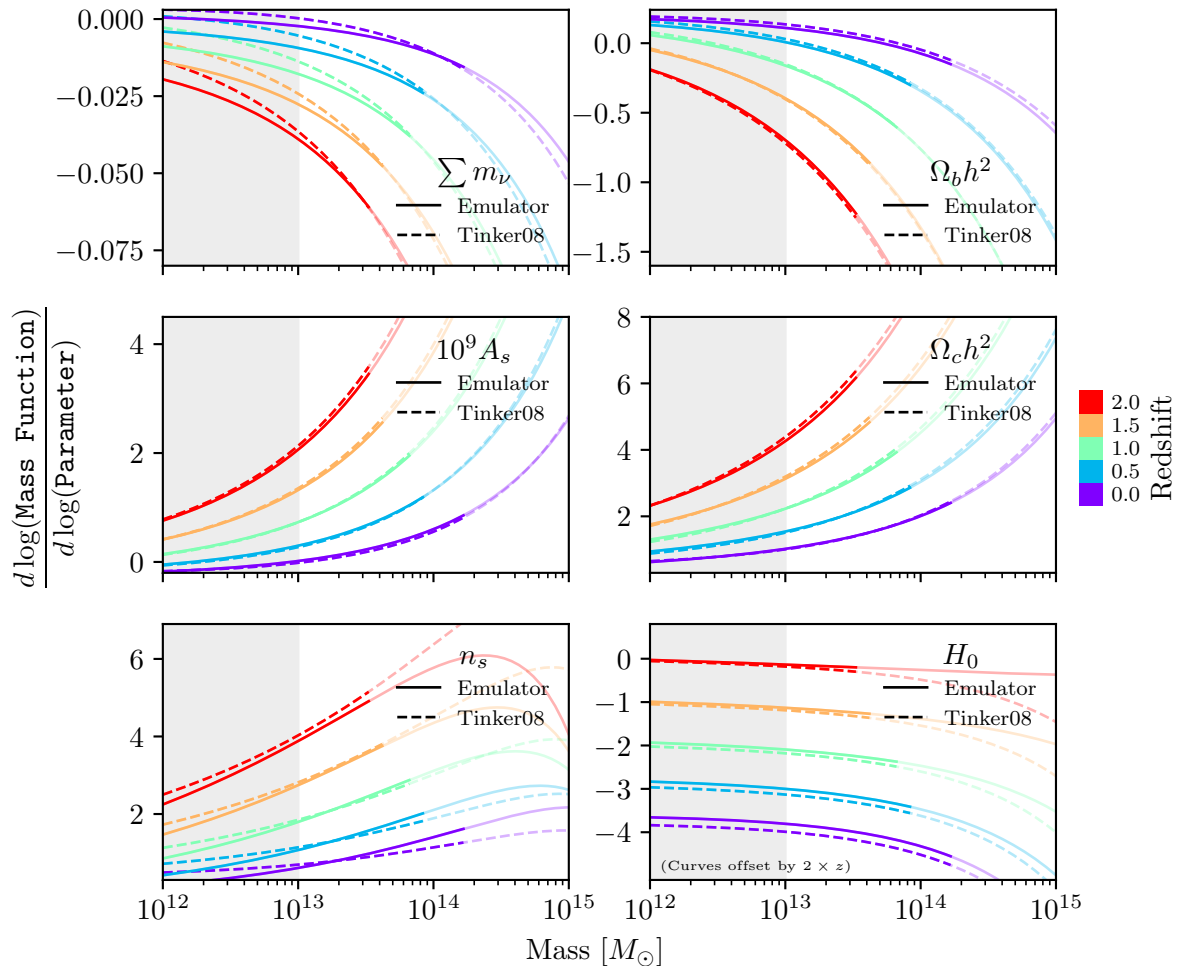


Figure 6. For a high S8 (Planck [111]) cosmology, the logarithmic derivative of the mass function with respect to cosmological parameters, and specifically n_s , significantly changes between our non-universal halo mass function emulator (solid) and the standard universal Tinker mass function [52] modified to depend on only the CDM and baryon content [83–85] (dashed) in the mass range where we have a significant number of halos to consider within our simulation (darker). This can be compared to a low S8 (DES Y3) cosmology shown in Fig. 7, where the logarithmic derivatives differ less between our halo mass function emulator and the Tinker mass function. The difference in cosmology dependence of the halo mass function in a low or high S8 cosmology is because more clusters exist in a high S8 cosmology. Therefore, the halo mass function on cluster mass scales has a greater dynamic range, allowing for greater cosmology dependence and impact from non-universality. Lighter parts of the lines correspond to where the jackknifed error on cluster abundance measurements from our simulations exceeds 1%, and the light grey region corresponds to the region that is $\lesssim 200 \times M_{\text{particle}}$.

Low S8 (DES Y3) Cosmology

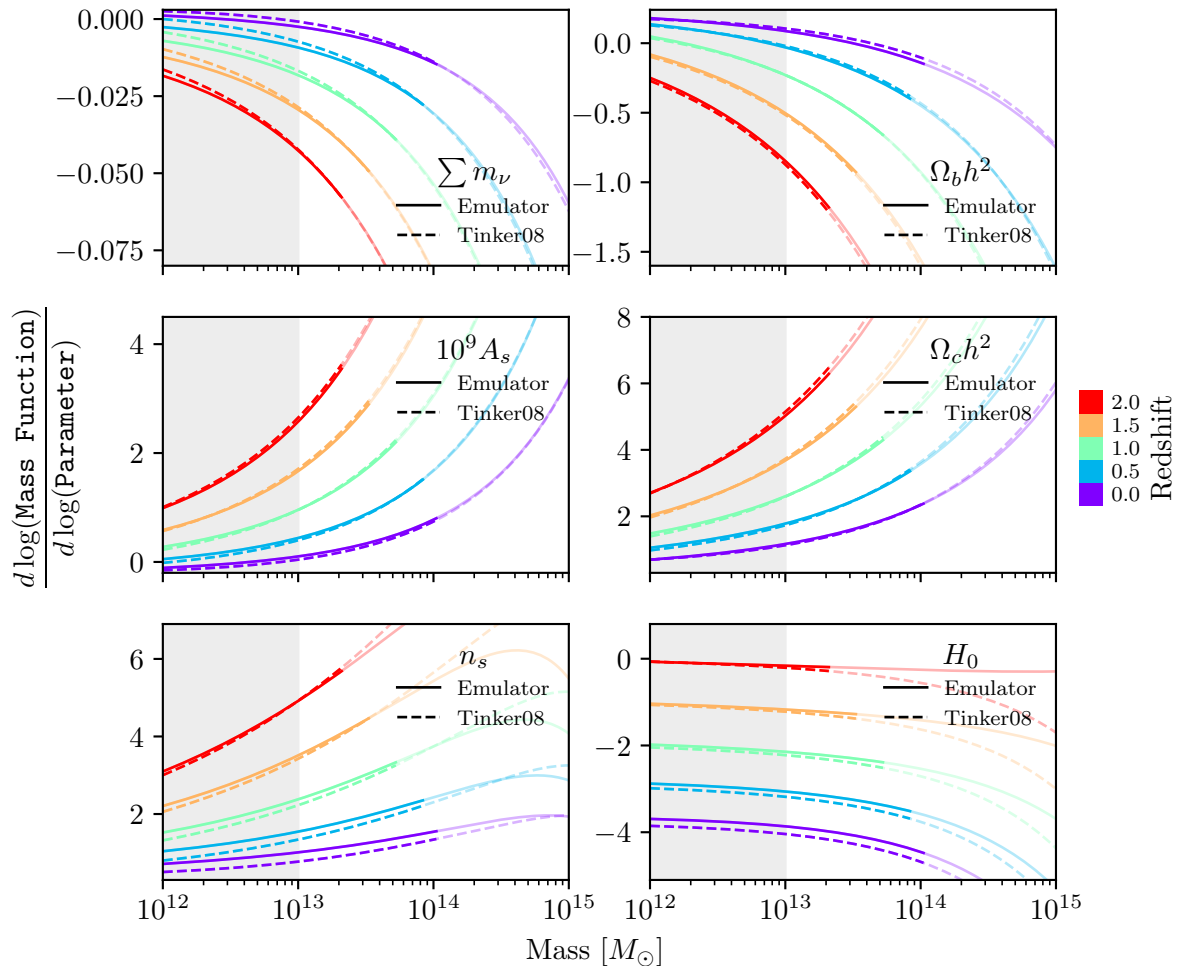


Figure 7. For a low S8 (DES Y3 [114]) cosmology, the logarithmic derivative of the mass function with respect to cosmological parameters does not change significantly between our non-universal halo mass function emulator (solid) and the standard universal Tinker mass function [52] modified to depend on only the CDM and baryon content [83–85] (dashed) in the mass range where we have a significant number of halos to consider within our simulation (darker). This can be compared to a high S8 (Planck) cosmology shown in Fig. 6, where the logarithmic derivatives differ much more between our halo mass function emulator and the Tinker mass function. The difference in cosmology dependence of the halo mass function in a low or high S8 cosmology is because more clusters exist in a high S8 cosmology. Therefore, the halo mass function on cluster mass scales has a greater dynamic range, allowing for greater cosmology dependence and impact from non-universality. Lighter parts of the lines correspond to where the jackknifed error on cluster abundance measurements from our simulations exceeds 1%, and the light grey region corresponds to the region that is $\lesssim 200 \times M_{\text{particle}}$.

and precision of our emulator are of most interest. Because of this, our performance plots throughout this paper have been restricted to only performance on the tier 2 simulations. In Fig. 8, we plot the absolute fractional error of the fits versus the actual measured mass function for all the simulations. This is the generalization of Fig. 2. In Fig. 9, we plot the absolute fractional error between the prediction of an emulator trained on all but one box versus the measured abundances Eq. (2.4) of that left-out box for all the simulations. This is the generalization of Fig. 3.

References

- [1] Z. Haiman, J.J. Mohr and G.P. Holder, *Constraints on Cosmological Parameters from Future Galaxy Cluster Surveys*, *Astrophys. J.* **553** (2001) 545 [[astro-ph/0002336](#)].
- [2] G. Holder, Z. Haiman and J. Mohr, *Constraints on ω_m , ω_l , and σ_8 , from galaxy cluster redshift distributions*, *Astrophys. J. Lett.* **560** (2001) L111 [[astro-ph/0105396](#)].
- [3] J. Weller, R. Battye and R. Kneissl, *Constraining dark energy with Sunyaev-Zeldovich cluster surveys*, *Phys. Rev. Lett.* **88** (2002) 231301 [[astro-ph/0110353](#)].
- [4] A. Albrecht et al., *Report of the Dark Energy Task Force*, [astro-ph/0609591](#).
- [5] S.W. Allen, A.E. Evrard and A.B. Mantz, *Cosmological Parameters from Observations of Galaxy Clusters*, *Ann. Rev. Astron. & Astrophys.* **49** (2011) 409 [[1103.4829](#)].
- [6] D.H. Weinberg, M.J. Mortonson, D.J. Eisenstein, C. Hirata, A.G. Riess and E. Rozo, *Observational probes of cosmic acceleration*, *Phys. Rep.* **530** (2013) 87 [[1201.2434](#)].
- [7] A.B. Mantz et al., *Weighing the giants – IV. Cosmology and neutrino mass*, *Mon. Not. Roy. Astron. Soc.* **446** (2015) 2205 [[1407.4516](#)].
- [8] S. Dodelson, K. Heitmann, C. Hirata, K. Honscheid, A. Roodman, U. Seljak et al., *Cosmic Visions Dark Energy: Science*, [1604.07626](#).
- [9] SPT collaboration, *Cluster Cosmology Constraints from the 2500 deg² SPT-SZ Survey: Inclusion of Weak Gravitational Lensing Data from Magellan and the Hubble Space Telescope*, *Astrophys. J.* **878** (2019) 55 [[1812.01679](#)].
- [10] DES collaboration, *Methods for cluster cosmology and application to the SDSS in preparation for DES Year 1 release*, *Mon. Not. Roy. Astron. Soc.* **488** (2019) 4779 [[1810.09456](#)].
- [11] I.n. Zubeldia and A. Challinor, *Cosmological constraints from Planck galaxy clusters with CMB lensing mass bias calibration*, *Mon. Not. Roy. Astron. Soc.* **489** (2019) 401 [[1904.07887](#)].
- [12] DES collaboration, *Combination of cluster number counts and two-point correlations: validation on mock Dark Energy Survey*, *Mon. Not. Roy. Astron. Soc.* **502** (2021) 4093 [[2008.10757](#)].
- [13] A. Mazoun, S. Bocquet, M. Garny, J.J. Mohr, H. Rubira and S.M.L. Vogt, *Probing interacting dark sector models with future weak lensing-informed galaxy cluster abundance constraints from SPT-3G and CMB-S4*, [2312.17622](#).
- [14] DES, SPT collaboration, *SPT Clusters with DES and HST Weak Lensing. II. Cosmological Constraints from the Abundance of Massive Halos*, [2401.02075](#).
- [15] DES collaboration, *The Dark Energy Survey*, [astro-ph/0510346](#).
- [16] DES collaboration, *Weak-lensing mass calibration of redMaPPer galaxy clusters in Dark Energy Survey Science Verification data*, *Mon. Not. Roy. Astron. Soc.* **469** (2017) 4899 [[1610.06890](#)].

Residuals of the Halo Mass Function Fits

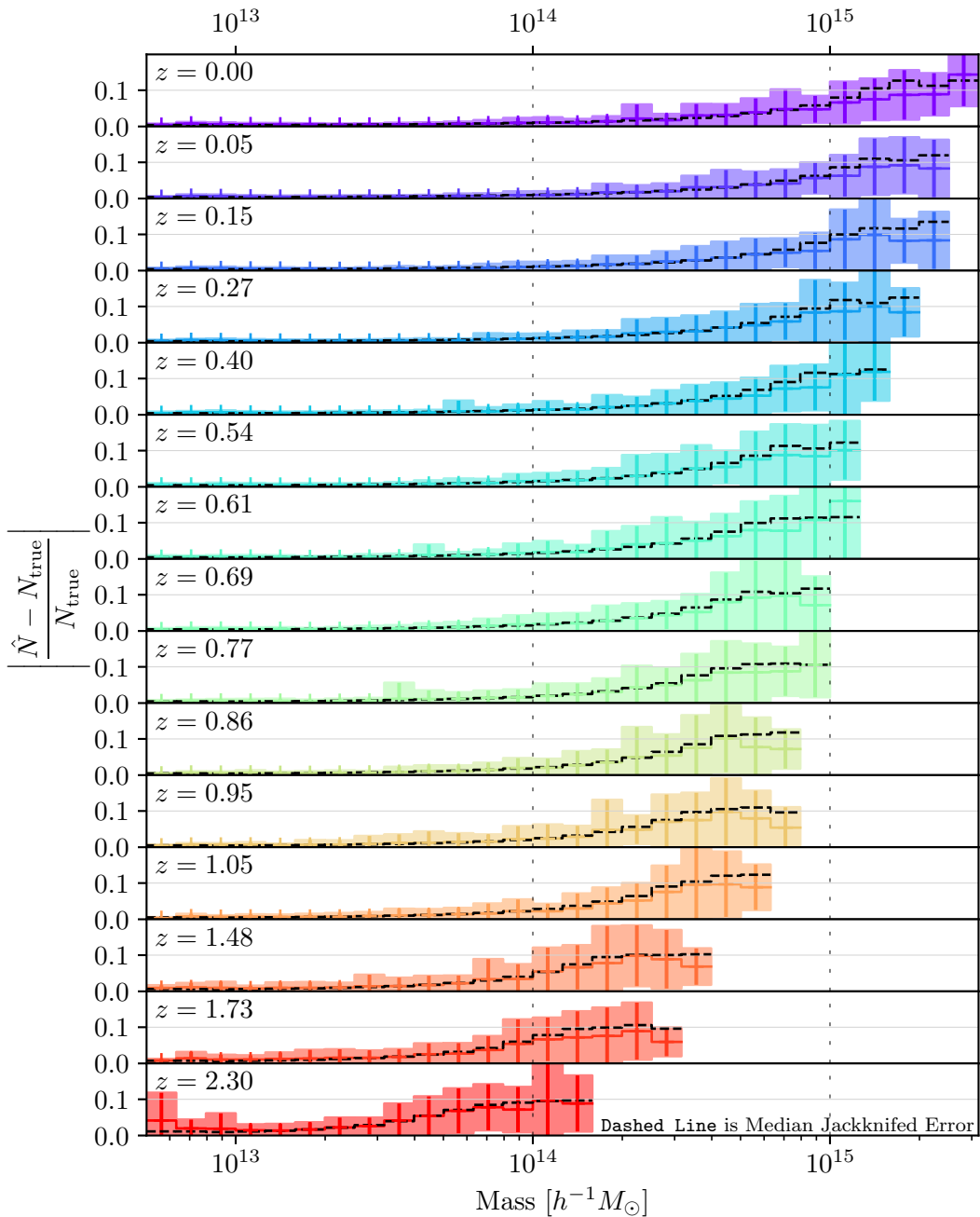


Figure 8. The absolute fractional error on halo abundance from our fits (colored) compared to the median jackknifed error (dashed black) in a given mass bin. This plot is analogous to Fig. 2 but for the whole suite of simulations instead of the tier 2 simulations that are of primary interest. Bands correspond to $\pm 1\sigma$ from the mean.

Residuals of the Halo Mass Function **Emulator**

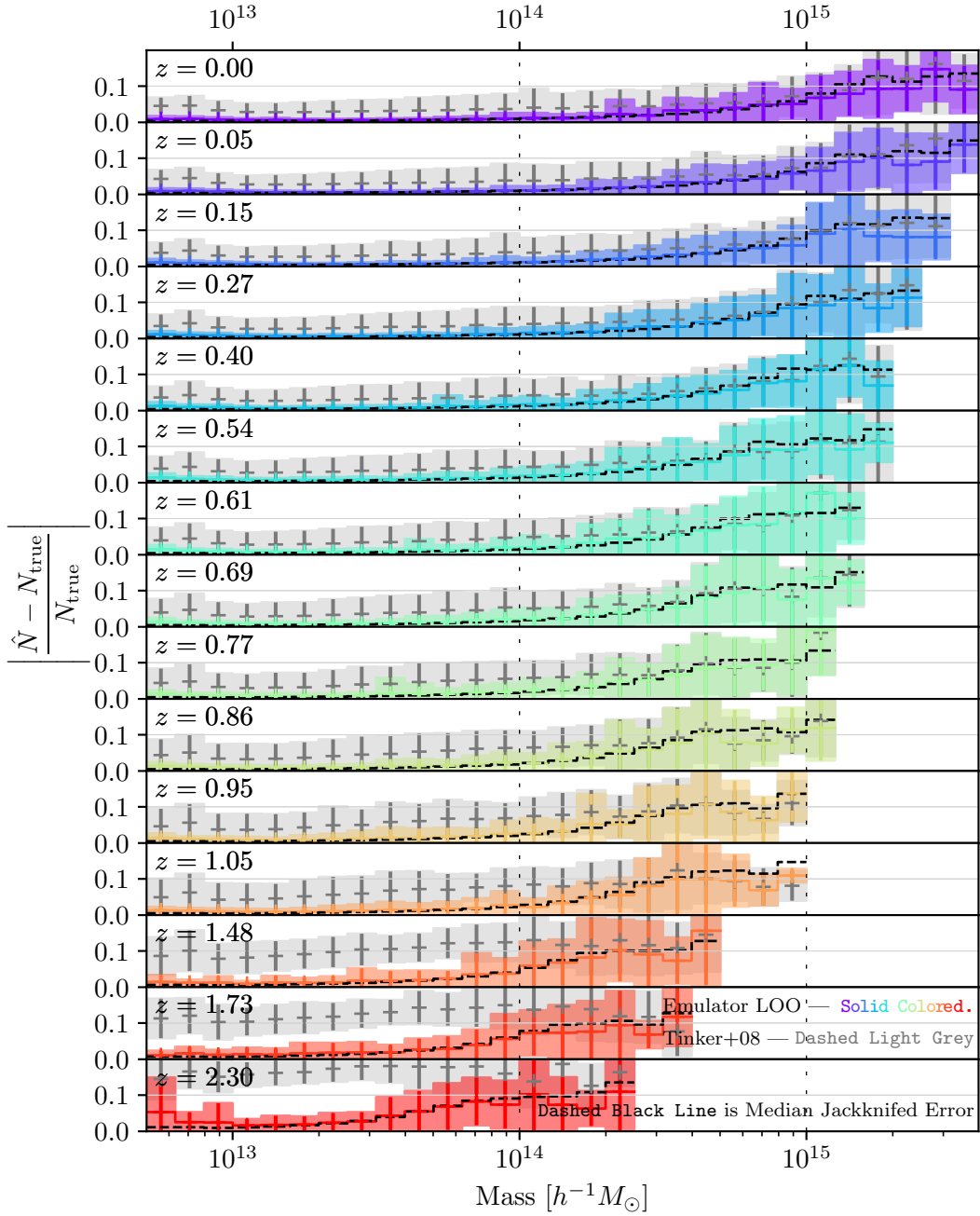


Figure 9. The absolute fractional error on halo abundance for a given box from our emulator architecture emulator trained on all but that box (colored) compared to the median jackknifed error (dashed black) and error of the Tinker halo mass function modified to depend only on CDM and baryons [83–85] (light grey) in a given mass bin. This plot is analogous to Fig. 3 but for the whole suite of simulations instead of the tier 2 simulations that are of primary interest. Bands correspond to $\pm 1\sigma$ from the mean.

- [17] DES collaboration, *The Dark Energy Survey: more than dark energy – an overview*, *Mon. Not. Roy. Astron. Soc.* **460** (2016) 1270 [[1601.00329](#)].
- [18] DES collaboration, *Dark Energy Survey Year 1 Results: Cosmological Constraints from Cluster Abundances, Weak Lensing, and Galaxy Correlations*, *Phys. Rev. Lett.* **126** (2021) 141301 [[2010.01138](#)].
- [19] H. Aihara et al., *First Data Release of the Hyper Suprime-Cam Subaru Strategic Program*, *Publ. Astron. Soc. Jap.* **70** (2018) S8 [[1702.08449](#)].
- [20] T. Sunayama et al., *Optical Cluster Cosmology with SDSS redMaPPer clusters and HSC-Y3 lensing measurements*, [2309.13025](#).
- [21] G.F. Lesci et al., *AMICO galaxy clusters in KiDS-DR3: Constraints on cosmological parameters and on the normalisation of the mass-richness relation from clustering*, *Astron. Astrophys.* **665** (2022) A100 [[2203.07398](#)].
- [22] R. Piffaretti, M. Arnaud, G.W. Pratt, E. Pointecouteau and J.B. Melin, *The MCXC: a meta-catalogue of x-ray detected clusters of galaxies*, *Astron. Astrophys.* **534** (2011) A109 [[1007.1916](#)].
- [23] H. Boehringer et al., *The rosat-eso flux limited x-ray (reflex) galaxy cluster survey I: the construction of the cluster sample*, *Astron. Astrophys.* **369** (2001) 826 [[astro-ph/0012266](#)].
- [24] R.A. Burenin, A. Vikhlinin, A. Hornstrup, H. Ebeling, H. Quintana and A. Mescheryakov, *The 400 square degrees ROSAT PSPC galaxy cluster survey: Catalog and statistical calibration*, *Astrophys. J. Suppl.* **172** (2007) 561 [[astro-ph/0610739](#)].
- [25] F. Pacaud et al., *The XXL Survey. II. The bright cluster sample: catalogue and luminosity function*, *Astron. Astrophys.* **592** (2016) A2 [[1512.04264](#)].
- [26] V. Ghirardini et al., *The SRG/eROSITA All-Sky Survey: Cosmology Constraints from Cluster Abundances in the Western Galactic Hemisphere*, [2402.08458](#).
- [27] E. Bulbul et al., *The SRG/eROSITA All-Sky Survey: The first catalog of galaxy clusters and groups in the Western Galactic Hemisphere*, [2402.08452](#).
- [28] SPT collaboration, *Galaxy Clusters Discovered via the Sunyaev-Zel'dovich Effect in the 2500-square-degree SPT-SZ survey*, *Astrophys. J. Suppl.* **216** (2015) 27 [[1409.0850](#)].
- [29] PLANCK collaboration, *Planck 2015 results. XXVII. The Second Planck Catalogue of Sunyaev-Zeldovich Sources*, *Astron. Astrophys.* **594** (2016) A27 [[1502.01598](#)].
- [30] ACT collaboration, *The Atacama Cosmology Telescope: The Two-Season ACTPol Sunyaev-Zel'dovich Effect Selected Cluster Catalog*, *Astrophys. J. Suppl.* **235** (2018) 20 [[1709.05600](#)].
- [31] SPT, DES collaboration, *The SPTpol Extended Cluster Survey*, *Astrophys. J. Suppl.* **247** (2020) 25 [[1910.04121](#)].
- [32] ACT, DES collaboration, *The Atacama Cosmology Telescope: A Catalog of >4000 Sunyaev-Zel'dovich Galaxy Clusters*, *Astrophys. J. Suppl.* **253** (2021) 3 [[2009.11043](#)].
- [33] S. Raghunathan, N. Whitehorn, M.A. Alvarez, H. Aung, N. Battaglia, G.P. Holder et al., *Constraining Cluster Virialization Mechanism and Cosmology Using Thermal-SZ-selected Clusters from Future CMB Surveys*, *Astrophys. J.* **926** (2022) 172 [[2107.10250](#)].
- [34] SPT, DES collaboration, *SPT-SZ MCMF: An extension of the SPT-SZ catalog over the DES region*, [2309.09908](#).
- [35] SPT, DES collaboration, *Galaxy Clusters Discovered via the Thermal Sunyaev-Zel'dovich Effect in the 500-square-degree SPTpol Survey*, [2311.07512](#).
- [36] LSST DARK ENERGY SCIENCE collaboration, *Large Synoptic Survey Telescope: Dark Energy Science Collaboration*, [1211.0310](#).

- [37] L. Amendola et al., *Cosmology and fundamental physics with the Euclid satellite*, *Living Rev. Rel.* **21** (2018) 2 [1606.00180].
- [38] SIMONS OBSERVATORY collaboration, *The Simons Observatory: Science goals and forecasts*, *JCAP* **02** (2019) 056 [1808.07445].
- [39] W.H. Press and P. Schechter, *Formation of galaxies and clusters of galaxies by selfsimilar gravitational condensation*, *Astrophys. J.* **187** (1974) 425.
- [40] J.R. Bond, S. Cole, G. Efstathiou and N. Kaiser, *Excursion set mass functions for hierarchical Gaussian fluctuations*, *Astrophys. J.* **379** (1991) 440.
- [41] R.K. Sheth and G. Tormen, *Large scale bias and the peak background split*, *Mon. Not. Roy. Astron. Soc.* **308** (1999) 119 [astro-ph/9901122].
- [42] R.K. Sheth, H.J. Mo and G. Tormen, *Ellipsoidal collapse and an improved model for the number and spatial distribution of dark matter haloes*, *Mon. Not. Roy. Astron. Soc.* **323** (2001) 1 [astro-ph/9907024].
- [43] A. Jenkins, C.S. Frenk, S.D.M. White, J.M. Colberg, S. Cole, A.E. Evrard et al., *The Mass function of dark matter halos*, *Mon. Not. Roy. Astron. Soc.* **321** (2001) 372 [astro-ph/0005260].
- [44] VIRGO collaboration, *Galaxy clusters in Hubble volume simulations: Cosmological constraints from sky survey populations*, *Astrophys. J.* **573** (2002) 7 [astro-ph/0110246].
- [45] M.S. Warren, K. Abazajian, D.E. Holz and L. Teodoro, *Precision determination of the mass function of dark matter halos*, *Astrophys. J.* **646** (2006) 881 [astro-ph/0506395].
- [46] K. Heitmann, Z. Lukic, S. Habib and P.M. Ricker, *Capturing halos at high redshifts*, *Astrophys. J. Lett.* **642** (2006) L85 [astro-ph/0601233].
- [47] B. Diemer, *Universal at last? The splashback mass function of dark matter halos*, *Astrophys. J.* **903** (2020) 87 [2007.10346].
- [48] EUCLID collaboration, *Euclid preparation. XXIV. Calibration of the halo mass function in $\Lambda(\nu)$ CDM cosmologies*, *Astron. Astrophys.* **671** (2023) A100 [2208.02174].
- [49] D. Reed, R. Bower, C. Frenk, A. Jenkins and T. Theuns, *The halo mass function from the dark ages through the present day*, *Mon. Not. Roy. Astron. Soc.* **374** (2007) 2 [astro-ph/0607150].
- [50] Z. Lukic, K. Heitmann, S. Habib, S. Bashinsky and P.M. Ricker, *The Halo Mass Function: High Redshift Evolution and Universality*, *Astrophys. J.* **671** (2007) 1160 [astro-ph/0702360].
- [51] J.D. Cohn and M.J. White, *Dark matter halo abundances, clustering and assembly histories at high redshift*, *Mon. Not. Roy. Astron. Soc.* **385** (2008) 2025 [0706.0208].
- [52] J.L. Tinker, A.V. Kravtsov, A. Klypin, K. Abazajian, M.S. Warren, G. Yepes et al., *Toward a halo mass function for precision cosmology: The Limits of universality*, *Astrophys. J.* **688** (2008) 709 [0803.2706].
- [53] J. Courtin, Y. Rasera, J.M. Alimi, P.S. Corasaniti, V. Boucher and A. Fuzfa, *Imprints of dark energy on cosmic structure formation: II) Non-Universality of the halo mass function*, *Mon. Not. Roy. Astron. Soc.* **410** (2011) 1911 [1001.3425].
- [54] M. Crocce, P. Fosalba, F.J. Castander and E. Gaztañaga, *Simulating the Universe with MICE: the abundance of massive clusters*, *Mon. Not. R. Astron. Soc.* **403** (2010) 1353 [0907.0019].
- [55] S. Bhattacharya, K. Heitmann, M. White, Z. Lukić, C. Wagner and S. Habib, *Mass Function Predictions Beyond Λ CDM*, *Astrophys. J.* **732** (2011) 122 [1005.2239].
- [56] E. Lawrence, K. Heitmann, M. White, D. Higdon, C. Wagner, S. Habib et al., *The Coyote Universe. III. Simulation Suite and Precision Emulator for the Nonlinear Matter Power Spectrum*, *Astrophys. J.* **713** (2010) 1322 [0912.4490].

- [57] K. Heitmann, E. Lawrence, J. Kwan, S. Habib and D. Higdon, *The Coyote Universe Extended: Precision Emulation of the Matter Power Spectrum*, *Astrophys. J.* **780** (2014) 111 [1304.7849].
- [58] E. Lawrence, K. Heitmann, J. Kwan, A. Upadhye, D. Bingham, S. Habib et al., *The Mira-Titan Universe II: Matter Power Spectrum Emulation*, *Astrophys. J.* **847** (2017) 50 [1705.03388].
- [59] EUCLID collaboration, *Euclid preparation: IX. EuclidEmulator2 – power spectrum emulation with massive neutrinos and self-consistent dark energy perturbations*, *Mon. Not. Roy. Astron. Soc.* **505** (2021) 2840 [2010.11288].
- [60] K.R. Moran, K. Heitmann, E. Lawrence, S. Habib, D. Bingham, A. Upadhye et al., *The Mira-Titan Universe – IV. High-precision power spectrum emulation*, *Mon. Not. Roy. Astron. Soc.* **520** (2023) 3443 [2207.12345].
- [61] J. DeRose, N. Kokron, A. Banerjee, S.-F. Chen, M. White, R. Wechsler et al., *Aemulus ν : precise predictions for matter and biased tracer power spectra in the presence of neutrinos*, *JCAP* **07** (2023) 054 [2303.09762].
- [62] T. Nishimichi et al., *Dark Quest. I. Fast and Accurate Emulation of Halo Clustering Statistics and Its Application to Galaxy Clustering*, *Astrophys. J.* **884** (2019) 29 [1811.09504].
- [63] T. McClintock, E. Rozo, A. Banerjee, M.R. Becker, J. DeRose, S. McLaughlin et al., *The Aemulus Project IV: Emulating Halo Bias*, [1907.13167](#).
- [64] B.D. Wibking, A.N. Salcedo, D.H. Weinberg, L.H. Garrison, D. Ferrer, J. Tinker et al., *Emulating galaxy clustering and galaxy-galaxy lensing into the deeply non-linear regime: methodology, information, and forecasts*, *Mon. Not. R. Astron. Soc.* **484** (2019) 989 [1709.07099].
- [65] A.N. Salcedo, A.H. Maller, A.A. Berlind, M. Sinha, C.K. McBride, P.S. Behroozi et al., *Spatial clustering of dark matter haloes: secondary bias, neighbour bias, and the influence of massive neighbours on halo properties*, *Mon. Not. R. Astron. Soc.* **475** (2018) 4411 [1708.08451].
- [66] Z. Zhai, J.L. Tinker, M.R. Becker, J. DeRose, Y.-Y. Mao, T. McClintock et al., *The Aemulus Project. III. Emulation of the Galaxy Correlation Function*, *Astrophys. J.* **874** (2019) 95 [1804.05867].
- [67] J.U. Lange, A.P. Hearin, A. Leauthaud, F.C. van den Bosch, H. Guo and J. DeRose, *Five per cent measurements of the growth rate from simulation-based modelling of redshift-space clustering in BOSS LOWZ*, *Mon. Not. R. Astron. Soc.* **509** (2022) 1779 [2101.12261].
- [68] N. Kokron, J. DeRose, S.-F. Chen, M. White and R.H. Wechsler, *The cosmology dependence of galaxy clustering and lensing from a hybrid N -body-perturbation theory model*, *Mon. Not. Roy. Astron. Soc.* **505** (2021) 1422 [2101.11014].
- [69] M. Zennaro, R.E. Angulo, M. Pellejero-Ibáñez, J. Stücker, S. Contreras and G. Aricò, *The BACCO simulation project: biased tracers in real space*, *Mon. Not. Roy. Astron. Soc.* **524** (2023) 2407 [2101.12187].
- [70] M. Pellejero-Ibanez, J. Stuecker, R.E. Angulo, M. Zennaro, S. Contreras and G. Arico, *Modelling galaxy clustering in redshift space with a Lagrangian bias formalism and N -body simulations*, *Mon. Not. Roy. Astron. Soc.* **514** (2022) 3993 [2109.08699].
- [71] B. Hadzhiyska, C. García-García, D. Alonso, A. Nicola and A. Slosar, *Hefty enhancement of cosmological constraints from the DES Y1 data using a hybrid effective field theory approach to galaxy bias*, *JCAP* **09** (2021) 020 [2103.09820].
- [72] K. Storey-Fisher, J. Tinker, Z. Zhai, J. DeRose, R.H. Wechsler and A. Banerjee, *The Aemulus Project VI: Emulation of beyond-standard galaxy clustering statistics to improve cosmological constraints*, *arXiv e-prints* (2022) arXiv:2210.03203 [2210.03203].

- [73] G. Valogiannis and C. Dvorkin, *Going beyond the galaxy power spectrum: An analysis of BOSS data with wavelet scattering transforms*, *Phys. Rev. D* **106** (2022) 103509 [2204.13717].
- [74] G. Valogiannis, S. Yuan and C. Dvorkin, *Precise Cosmological Constraints from BOSS Galaxy Clustering with a Simulation-Based Emulator of the Wavelet Scattering Transform*, **2310.16116**.
- [75] T. McClintock, E. Rozo, M.R. Becker, J. DeRose, Y.-Y. Mao, S. McLaughlin et al., *The Aemulus Project II: Emulating the Halo Mass Function*, *Astrophys. J.* **872** (2019) 53 [1804.05866].
- [76] S. Bocquet, K. Heitmann, S. Habib, E. Lawrence, T. Uram, N. Frontiere et al., *The Mira-Titan Universe. III. Emulation of the Halo Mass Function*, *Astrophys. J.* **901** (2020) 5 [2003.12116].
- [77] C.E. Rasmussen and C.K.I. Williams, *Gaussian Processes for Machine Learning*, The MIT Press (11, 2005), 10.7551/mitpress/3206.001.0001.
- [78] I. Sobol', *On the distribution of points in a cube and the approximate evaluation of integrals*, *USSR Computational Mathematics and Mathematical Physics* **7** (1967) 86.
- [79] M. Michaux, O. Hahn, C. Rampf and R.E. Angulo, *Accurate initial conditions for cosmological N-body simulations: minimizing truncation and discreteness errors*, *Mon. Not. R. Astron. Soc.* **500** (2021) 663 [2008.09588].
- [80] W. Elbers, C.S. Frenk, A. Jenkins, B. Li and S. Pascoli, *An optimal non-linear method for simulating relic neutrinos*, *Mon. Not. Roy. Astron. Soc.* **507** (2021) 2614 [2010.07321].
- [81] P.S. Behroozi, R.H. Wechsler and H.-Y. Wu, *The ROCKSTAR Phase-space Temporal Halo Finder and the Velocity Offsets of Cluster Cores*, *Astrophys. J.* **762** (2013) 109 [1110.4372].
- [82] W. Hu and A.V. Kravtsov, *Sample variance considerations for cluster surveys*, *Astrophys. J.* **584** (2003) 702 [astro-ph/0203169].
- [83] K. Ichiki and M. Takada, *The impact of massive neutrinos on the abundance of massive clusters*, *Phys. Rev. D* **85** (2012) 063521 [1108.4688].
- [84] F. Villaescusa-Navarro, F. Marulli, M. Viel, E. Branchini, E. Castorina, E. Sefusatti et al., *Cosmology with massive neutrinos I: towards a realistic modeling of the relation between matter, haloes and galaxies*, *JCAP* **03** (2014) 011 [1311.0866].
- [85] M. Costanzi, F. Villaescusa-Navarro, M. Viel, J.-Q. Xia, S. Borgani, E. Castorina et al., *Cosmology with massive neutrinos III: the halo mass function and an application to galaxy clusters*, *JCAP* **12** (2013) 012 [1311.1514].
- [86] D. Blas, J. Lesgourgues and T. Tram, *The Cosmic Linear Anisotropy Solving System (CLASS). Part II: Approximation schemes*, *Journal of Cosmology and Astro-Particle Physics* **2011** (2011) 034 [1104.2933].
- [87] J. Lesgourgues and T. Tram, *The Cosmic Linear Anisotropy Solving System (CLASS) IV: efficient implementation of non-cold relics*, *Journal of Cosmology and Astro-Particle Physics* **2011** (2011) 032 [1104.2935].
- [88] A. Cooray and R.K. Sheth, *Halo Models of Large Scale Structure*, *Phys. Rept.* **372** (2002) 1 [astro-ph/0206508].
- [89] O. Borůvka, *O jistém problému minimálním*, *Práce Moravské Přírodovědecké Společnosti* **3** (1926) 37–58.
- [90] J.B. Kruskal, *On the shortest spanning subtree of a graph and the traveling salesman problem*, *Proceedings of the American Mathematical Society* **7** (1956) 48.

- [91] R.C. Prim, *Shortest connection networks and some generalizations*, *The Bell System Technical Journal* **36** (1957) 1389.
- [92] H. Loberman and A. Weinberger, *Formal procedures for connecting terminals with a minimum total wire length*, *J. ACM* **4** (1957) 428–437.
- [93] E.W. Dijkstra, *A note on two problems in connexion with graphs*, *Numer. Math.* **1** (1959) 269–271.
- [94] B. Matern, *Spatial Variation*, Lecture Notes in Statistics, Springer New York (2013).
- [95] M. Stein, *Interpolation of Spatial Data: Some Theory for Kriging*, Springer Series in Statistics, Springer New York (2012).
- [96] E.V. Bonilla, K.M.A. Chai and C.K.I. Williams, *Multi-task gaussian process prediction*, in *Proceedings of the 20th International Conference on Neural Information Processing Systems*, NIPS’07, (Red Hook, NY, USA), p. 153–160, Curran Associates Inc., 2007.
- [97] J.R. Gardner, G. Pleiss, D. Bindel, K.Q. Weinberger and A.G. Wilson, *GPYtorch: Blackbox Matrix-Matrix Gaussian Process Inference with GPU Acceleration*, *arXiv e-prints* (2018) [arXiv:1809.11165](https://arxiv.org/abs/1809.11165) [[1809.11165](https://arxiv.org/abs/1809.11165)].
- [98] I. Loshchilov and F. Hutter, *Decoupled Weight Decay Regularization*, *arXiv e-prints* (2017) [arXiv:1711.05101](https://arxiv.org/abs/1711.05101) [[1711.05101](https://arxiv.org/abs/1711.05101)].
- [99] SDSS collaboration, *REDMAPPER I: Algorithm and SDSS DR8 Catalog*, *Astrophys. J.* **785** (2014) 104 [[1303.3562](https://arxiv.org/abs/1303.3562)].
- [100] N. Kaiser, *Evolution and clustering of rich clusters.*, *Mon. Not. R. Astron. Soc.* **222** (1986) 323.
- [101] R.A. Sunyaev and Y.B. Zeldovich, *Small-Scale Fluctuations of Relic Radiation*, *J. Plasma Physics* **7** (1970) 3.
- [102] E. Rozo, H.-Y. Wu and F. Schmidt, *Stacked Weak Lensing Mass Calibration: Estimators, Systematics, and Impact on Cosmological Parameter Constraints*, *Astrophys. J.* **735** (2011) 118 [[1009.0756](https://arxiv.org/abs/1009.0756)].
- [103] SPT collaboration, *Cluster mass calibration at high redshift: HST weak lensing analysis of 13 distant galaxy clusters from the South Pole Telescope Sunyaev–Zel’dovich Survey*, *Mon. Not. Roy. Astron. Soc.* **474** (2018) 2635 [[1611.03866](https://arxiv.org/abs/1611.03866)].
- [104] M. Simet, T. McClintock, R. Mandelbaum, E. Rozo, E. Rykoff, E. Sheldon et al., *Weak lensing measurement of the mass–richness relation of SDSS redMaPPer clusters*, *Mon. Not. Roy. Astron. Soc.* **466** (2017) 3103 [[1603.06953](https://arxiv.org/abs/1603.06953)].
- [105] R. Murata, T. Nishimichi, M. Takada, H. Miyatake, M. Shirasaki, S. More et al., *Constraints on the mass–richness relation from the abundance and weak lensing of SDSS clusters*, *Astrophys. J.* **854** (2018) 120 [[1707.01907](https://arxiv.org/abs/1707.01907)].
- [106] SPT collaboration, *Sunyaev–Zel’dovich effect and X-ray scaling relations from weak lensing mass calibration of 32 South Pole Telescope selected galaxy clusters*, *Mon. Not. Roy. Astron. Soc.* **483** (2019) 2871 [[1711.05344](https://arxiv.org/abs/1711.05344)].
- [107] DES collaboration, *Dark Energy Survey Year 1 Results: Weak Lensing Mass Calibration of redMaPPer Galaxy Clusters*, *Mon. Not. Roy. Astron. Soc.* **482** (2019) 1352 [[1805.00039](https://arxiv.org/abs/1805.00039)].
- [108] R. Murata, M. Oguri, T. Nishimichi, M. Takada, R. Mandelbaum, S. More et al., *The mass–richness relation of optically selected clusters from weak gravitational lensing and abundance with Subaru HSC first-year data*, [1904.07524](https://arxiv.org/abs/1904.07524).
- [109] LSST DARK ENERGY SCIENCE collaboration, *The LSST Dark Energy Science Collaboration (DESC) Science Requirements Document*, [1809.01669](https://arxiv.org/abs/1809.01669).

- [110] J. Towns, T. Cockerill, M. Dahan, I. Foster, K. Gaither, A. Grimshaw et al., *Xsede: Accelerating scientific discovery computing in science & engineering*, 16 (5): 62–74, sep 2014, URL <https://doi.org/10.1109/mcse> **128** (2014) .
- [111] PLANCK collaboration, *Planck 2018 results. VI. Cosmological parameters*, *Astron. Astrophys.* **641** (2020) A6 [[1807.06209](#)].
- [112] L. Ondaro-Mallea, R.E. Angulo, M. Zennaro, S. Contreras and G. Aricò, *Non-universality of the mass function: dependence on the growth rate and power spectrum shape*, *Mon. Not. Roy. Astron. Soc.* **509** (2021) 6077 [[2102.08958](#)].
- [113] N. Guo, L. Lucie-Smith, H.V. Peiris, A. Pontzen and D. Piras, *Deep learning insights into non-universality in the halo mass function*, [2405.15850](#).
- [114] DES collaboration, *Dark Energy Survey Year 3 results: Cosmological constraints from galaxy clustering and weak lensing*, *Phys. Rev. D* **105** (2022) 023520 [[2105.13549](#)].